universität wien

MASTERARBEIT / MASTER'S THESIS

Titel der Masterarbeit / Title of the Master's Thesis

Derivation, Analysis and Simulations of a Model for Tethered Leukocytes

verfasst von / submitted by

Laura Maria Kanzler, BSc

angestrebter akademischer Grad / in partial fulfilment of the requirements for the degree of

Master of Science (MSc)

Wien, 2017 / Vienna, 2017

Studienkennzahl lt. Studienblatt / degree programme code as it appears on the student record sheet:	A 066 821
Studienrichtung lt. Studienblatt / degree programme as it appears on the student record sheet:	Masterstudium Mathematik
Betreut von / Supervisor:	Univ.-Prof. Dr. Christian Schmeiser

Abstract

It is well known that within the extravasation process, leukocytes roll along the blood vessel wall before they come to rest and are able to leave the bloodstream. In recent flow chamber experiments it was observed that during this process of rolling the leukocyte produces membrane tethers, which connect the cell with the vessel wall and slow down the movement of the leukocyte. This master's thesis deals with the modelling, analysis and numerical simulation of such membrane tethers.

In the first part of this work an overview of the biological background is given. This serves as basis for the modelling assumptions in part two, where the model for the tether is derived and then simplified.
In the third part the existence and uniqueness of a solution to the simplified model are investigated. The method established in this theoretical analysis, needing Banach's fixed-point theorem and other results from functional analysis, is also used to produce numerical simulations in the fourth part.

Zusammenfassung

Es ist bereits bekannt, dass bei dem Prozess der Leukodiapedese die Leukozyten erst entlang der Gefäßinnenwand rollen, bis sie zu Ruhe kommen und dann den Blutkreislauf durch die Gefäßwand verlassen können. Wie sich kürzlich in Flusskammer-Experimenten gezeigt hat, werden vom Leukozyten in der Phase des Rollens Membranausstülpungen mit sehr geringem Durchmesser, die sogenannten Tether, gebildet, die die Zelle mit dem Endothel verbinden und eine bremsende Wirkung haben. Diese Masterarbeit beschäftigt sich mit der Modellierung, Analysis, sowie mit numerischen Simulationen dieser Tether.

Im ersten Teil dieser Arbeit wird ein Überblick über den biologischen Hintergrund gegeben, was als Grundstein für die Modellierungsannahmen im zweiten Teil dient. Hier wird erst ein Model für den Tether entwickelt, das anschließend zu dem vereinfacht wird, was als Objekt der Analyse in den nächsten Kapiteln dient.
Der dritte Teil der Arbeit ist der Frage nach Existenz und Eindeutigkeit einer Lösung des Models gewidmet. Die Methode, die dabei genutzt wurde, verwendet den Banachschen Fixpuktsatz sowie weitere Resultate aus der Funktionalanalysis. Diese dient ebenfalls als Grundlage für die numerischen Simualtionen im vierten und letzten Teil der Arbeit.

Acknowledgments

First of all, I want to thank my advisor Prof. Christian Schmeiser for giving me with this topic the opportunity to learn under his guidance how to translate biological problems in mathematical ones and for never getting tired to answer my numerous questions.
Secondly, special thanks must got to my parents. Not only for their financial, but also for their moral support and for -after initial astonishment- always encouraging me in my decision to become a mathematician.
Furthermore, I am indebted to my cousin Vera Kargl, who read over my chapter about the biological background, and to my colleague Konstantin Weiner, who gave answer to some physical questions, which did arise within the modeling-part of this work.
Last but not least, I would like to show my gratitude to my colleagues and friends Sarah Henze, Annemarie Grass and Manveer Mangat for their support and numerous talks we had throughout the years of my studies.

Contents

Part 1. Introduction: Biological Background

White blood cells, also called *leukocytes*, belong to the immune system of vertebrates and are the crucial factor for protecting the body against pathogens, cancer cells, and other dangerous invaders. They are produced in bone marrow and can also be found in lymph channels and of course in the blood of vertebrates.
Since there are many types of aetiologic agents, also many types of leukocytes are needed to protect the body. These different types of white blood cells do not only vary in their function in the immune system, but also in their shape. One kind of leukocyte is the so called *neutrophil granulocyte*, which comprises the majority of the circulating white blood cells in human bodies and comes to action when inflammation due to bacterial or fungal infection occurs. In order to reach the site of an infection, they have to leave the blood stream. This process is called *leukocyte extravasation* and happens in several steps. The following description of the extravasation process of neutrophils is based on [7, 4, 3], where more biochemical details can be found.

1. Leukocyte Extravasation

Leukocyte recruitment from the blood into the affected tissue is needed in the process of inflammation, which is an acute response of the immune system when it comes to an infection. Neutrophil granulocytes are the first responder immune cells to be taken there. Their recruitment mostly takes place in postcapillary venules (venules following the capillaries) of the inflamed site. Extravasation is a chemotactic process and therefore initiated by chemical signals caused by the infection. Once the neutrophils detect these signals with molecules on their cell membrane and start following the chemical gradients of the chemoattractants, the following steps until extravasation can be observed: Rolling, adhesion, crawling, and finally transmigration (see 1).

Once a free circulating neutrophil detects chemical changes on the surface of the endothelium of vessels near the infection, it starts with the process of *tethering*. This means that selectin ligands on the cell membrane bind to selectins on the endothelial cells. This is modulated by integrins, which are transmenbrane receptors on the surface of the leukocyte. As soon as the connection to the vessel wall is provided, the neutrophils start *rolling* along the endothelium in the direction of the blood stream. At the points where the cell is connected to the venule wall, long sub-micron diameter tubes are pulled out of it. The so-called *tethers*. If the forces of the blood flow acting on the neutrophil are too strong, the bonds that anchor the tether to the cell wall might break, which is called tether breaking. It usually gives the granulocyte a push forward in the direction on the flowing blood. Also *slings* are formed. Other than tethers, which appear behind the cell, slings occur at the front.

During the process of rolling, other chemicals activate the integrins on the surface of the rolling cells. The now activated receptors cause stronger bindings instead of the former frail ones such that the movement of the

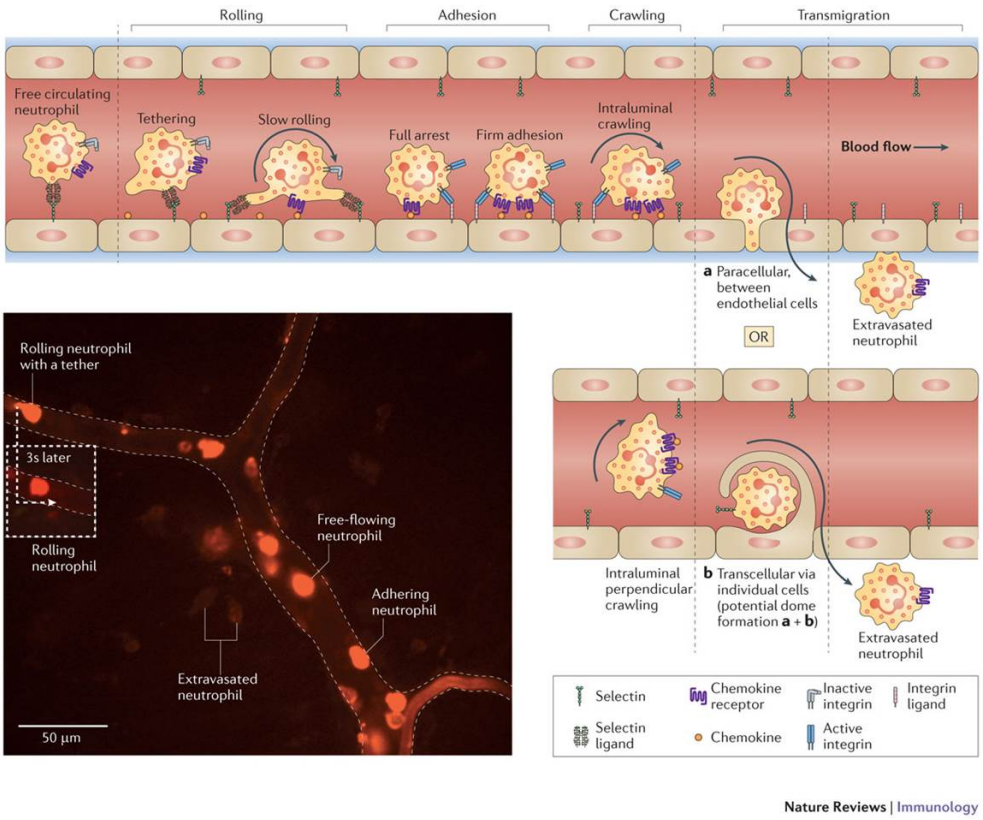

FIGURE 1. Steps of Neutrophil Extravasation [3]

rolling neutrophils becomes less until it comes to tight adhesion. One could think that the site of their arrest will then be the place, where the cells leave the blood stream. But unlike this, it was observed that most neutrophils were actively crawling in a small area around the adhesion spot, while on one hand beeing elonginated because of the shear stress caused by the blood flow, but on the other hand remaining firmly attached to the endothelium.

If a suitable spot on the vessel wall is found, the last step of extravasation starts, the so-called *transmission*. Two ways of neutrophils leaving the blood stream were observed. Either they leave paracellularly or transcellularly. If neutrophils choose the first possibility mentioned, then they wander between cells of the venule to the outside. It is also possible that they leave the blood stream by wandering through an endothelical cell. Which type of transmission of each granulocyte is chosen depends on some factors as the surface structure and the alignment of cells of the vessel wall and is not investigated that good at the moment.

After finally reaching the inflamated tissue, neutrophils start their work against the infection. Most of them will die in this process, are destroyed and cleared by macrophages (another type of white blood cells), gathered and end up as pus. Only in laboratory experiments and very seldom in

living beings reverse neutrophil migration has been observed.

2. Tether under Blood Flow

In this section a closer look at the tethers and their behavior under the forces acting on them during the rolling of neutrophils is taken. These information is taken from [4], where newest observations with mice neutrophil granulocytes in flow chamber experiments conducted by Ley et al. about tether and sling formation, tether breaking and tether-to-sling transition can be found.
Neutrophil granulocytes are capable of rolling at high shear stress, which among other things can on one hand be referred to the deformability of neutrophils and on the other hand to the formation of tethers and slings that sustain the loads of the forces.

As already stated above, tethers form during the rolling-part of neutrophil extravasation. Since some spots on the membrane of the leukocyte get well fixed at the vessel wall through chemical bindings, cell membrane is pulled out of the rolling neutrophil caused by hydrodynamic drag and tethers are formed. While one end of the long tube-like membrane excrescence with extremely small lumen is anchored at the venule wall, the other end at the cell serves as source for new membrane material when it is pulled longer during the process of rolling. Once formed, the tether does not only have to bear the pull from the leukocyte, but also the forces acting on it from the blood flow. Under high shear stress (greater than 0.6 Pa) it was observed that a neutrophil forms around 5 tethers of length between 1.2 μm and 30.1 μm. To visualize these descriptions, see 2. The first picture 2(a) shows a bottom view of rolling neutrophils with the blood streaming from left to right. The tethers at the rear of the cell cannot be seen, but their anchors at the wall occur as small glowing dots behind the granulocyte. Picture 2(b) captured neutrophils shortly after their arrest from rolling to the right. Since this is a side view image, tethers behind the cell can be seen clearly. To get a better spatial idea, image 2(c) shows a 3D reconstruction of a shortly resting neutrophil.
Under that many forces acting on tethers, the bindings anchoring them on the endothelium might break at some point. This leads to a forward microjump of the cell, which was witnessed in the experiments. Individual tethers participate significantly in preventing the cell from running with the flow, since it was even observed that after multiple consecutive tether breaks large granulocyte displacements followed. In 3 one can see such neutrophil displacement after several tether breaks. The white lines mark the front of the cell at different consecutive times, while the arrows show the anchor points of a tether in the last frame it was visible.
It was also observed that approximately 15% of all broken tethers in the rear of the neutrophil lead to the formation of slings in front of the cell. After a former tether is detached, the blood flow first maneuveres it to the wall before it is dragged in the front by the rolling of the cell. There, if the point of attachment gets close enough, it can bind again on the vessel wall and is

load bearing again. A tether-to-sling transition could only be observed at relatively long tethers. In 4 one can see the key frames of such a transition at a neutrophil which again is rolling from left to right. While in the first frame a tether can be seen clearly behind the granulocyte, the other frames show it as a sling in front of the cell which is able to bind to the wall after 1.2 seconds.

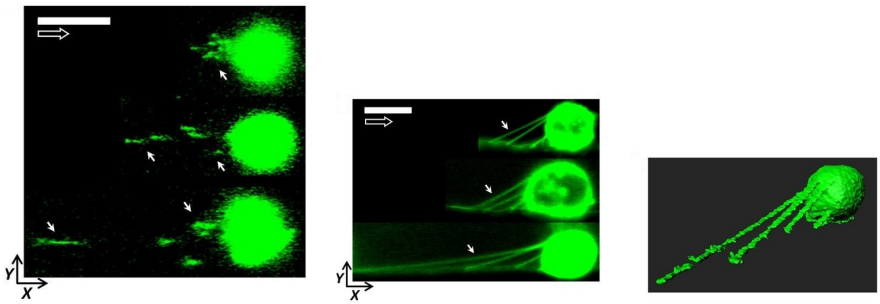

(a) Bottom view of rolling neutrophils

(b) Side view of just arrested neutrophils

(c) 3D reconstruction image of a recently arrested neutrophil

FIGURE 2. Microscope images of rolling and just arrested neutrophil granulocytes with tethers [4]

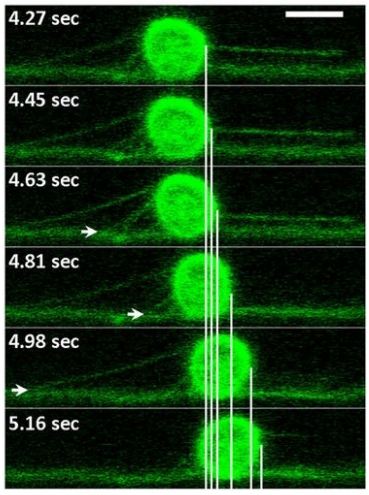

FIGURE 3. Tether breaks resulting in microjumps of the neutrophil [4]

Since in the whole process many physical forces and mechanical mechanisms are involved, the above described observations give also rise to some questions of physical and mathematical interest. A different, theoretical, approach is therefore useful for better understanding, predicting and confirming the witnessed observations from a non-biological point of view.

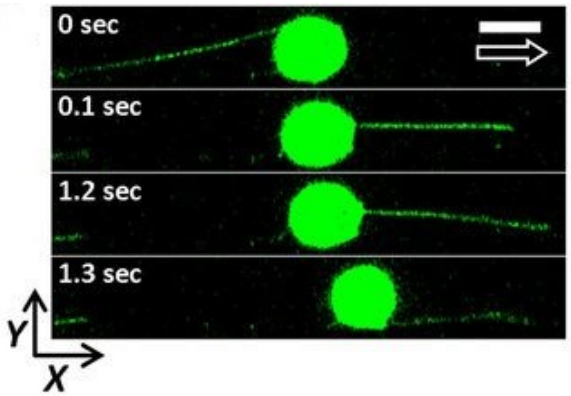

FIGURE 4. Side view tether-to-sling transition [4]

As a step in that direction, this work will present a mathematical model, which describes a tether of a rolling neutrophil acting under the forces originating from the blood flow.

Part 2. Modelling

With the biologocal background explained in the last chapter in mind, it is now time to approach the modelling of such a tether.

1. Assumptions and Setting

Inspired by some images from [4] of rolling neutrophils taken in the side view flow chamber, we consider the whole process in only two dimensions. One can imagine a cross section through a leukocyte exactly where a tether is pulled out of the cell surrounded by a two-dimensional laminar flow. This, in general, is a huge simplification for the actual three-dimensional objects. In our case, it is quite reasonable as the main movement of the neutrophil is one-dimensional and goes in the direction of the flow with only very small lateral displacement.

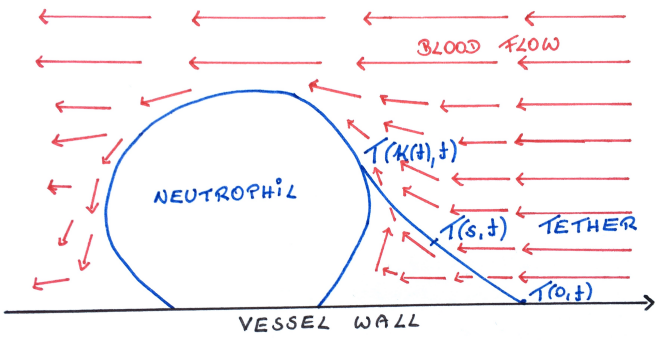

Figure 5. Sketch of the 2D-model

As visualized in 5, we are in $\mathbb{R}^2$ where the x-axis serves as, in our model of course only one-dimensional, vessel wall. The neutrophil granulocyte is placed on the x-axis and rolls in the direction of the blood flow from the right to the left. The blood flow is modelled as a two-dimensional laminar flow with velocity $\begin{pmatrix} \mathcal{U} \\ 0 \end{pmatrix}$, where $\mathcal{U}$ is set to be negative as we decided that the blood streams from the right to the left.
Biologically, it is quite reasonable to see the tether only as one-dimensional object, since as a sub-micron diameter tube its thickness is negligible compared to the other magnitudes in this process. Therefore, we now introduce the tether $\{T(s,t) : \ s \in [0, \kappa(t)]\} \subset \mathbb{R}^2$ as a one-dimensional curve in the plane, where $t > 0$ is the time, $s \in [0, \kappa(t)]$ is the parameter of the path $T(.,t)$ and has to be understood as Lagrangian-coordinate, which models the fact, that the tether consisting of cell membrane is not elastic. The time-dependent, positive function κ describes the length of the parameter interval. Furthermore, we assume that at time $t = 0$ the curve $T(.,0)$ is parametrized by arc-length, which is characterized by $|\frac{d}{ds}T(s,0)| = \sqrt{(\frac{d}{ds}T_1(s,0))^2 + (\frac{d}{ds}T_2(s,0))^2} = 1$, $\forall s \in [0, \kappa(0)]$. We cannot guarantee this

property of the path being maintained with proceeding time, but we assume

$$\kappa(t) = \int_0^{\kappa(t)} |\partial_s T(s,t)|\, ds, \quad \forall t > 0,$$

which implicates that the tangential vector is normalized at least on average and assures that the length of the parameter interval corresponds to the actual length of the curve. The Lagrangian-coordinate does not change at the anchored end of the tether, while the coordinate at the endpoint at the cell will vary in time. Therefore, we will for now use the convention that $s = \kappa(t)$ corresponds to the end of the tether at the neutrophil while at $s = 0$ the tether is anchored at the vessel wall.

In order to investigate the behavior of the tether, the curve given by T will be the unknown of our equations we will derive under consideration of the forces it has to bear.

2. Derivation of the Model

The model takes into account the bending and tension of the tether as well as friction between tether and blood. We consider a friction dominated model, where forces derived from a potential (bending and stretching) energy are balanced with friction forces. The potential energy is given by

$$E_{pot}[T] = \frac{1}{2}\int_0^{\kappa} \left(\mu|\partial_s^2 T|^2 + \zeta\kappa|\partial_s T|^2\right)\, ds\,.$$

The positive parameter μ is the *bending stiffness*, and the tension $\zeta\kappa$ with the parameter $\zeta > 0$ is assumed proportional to the length κ of the tether, modeling the assumption that bigger forces are required to pull longer tethers out of the leukocyte cell membrane.

The variation

$$\begin{aligned}\delta E_{pot}[T] = &\int_0^{\kappa} \left(\mu\partial_s^4 T - \zeta\kappa\partial_s^2 T\right)\cdot(\delta T)\, ds \\ &+ \mu\partial_s^2 T\cdot\partial_s(\delta T)\Big|_0^{\kappa} + \left(\zeta\kappa\partial_s T - \mu\partial_s^3 T\right)\cdot(\delta T)\Big|_0^{\kappa}\end{aligned}$$

provides both the force density $\mu\partial_s^4 T - \zeta\kappa\partial_s^2 T$ and boundary conditions for different situations. We shall always assume freely rotating boundaries, i.e.

$$\partial_s^2 T = 0 \qquad \text{for } s = 0, \kappa\,.$$

As a second boundary condition we use either *free boundaries*, i.e.

$$\zeta\kappa\partial_s T - \mu\partial_s^3 T = 0 \qquad \text{for } s = 0 \text{ and/or } s = \kappa\,,$$

or *prescribed endpoints*

$$T = T_0 \quad \text{for } s = 0\,, \qquad T = T_1 \quad \text{for } s = \kappa\,,$$

(implying $\delta T = 0$ for $s = 0, \kappa$).

The above mentioned force density is balanced with a friction force, where we assume different friction coefficients $\gamma^{\parallel} > 0$ and $\gamma^{\perp} > 0$ for the tangential

and, respectively, orthogonal components. This leads to the differential equation

(1)

$$-\mu\partial_s^4 T+\zeta\kappa\partial_s^2 T-\gamma^{\|}\frac{\partial_s T}{|\partial_s T|}\cdot(\partial_t T-v(T))\frac{\partial_s T}{|\partial_s T|}-\gamma^{\perp}\frac{\partial_s T^{\perp}}{|\partial_s T|}\cdot(\partial_t T-v(T))\frac{\partial_s T^{\perp}}{|\partial_s T|}=0,$$

where $\partial_t T - v(T)$ is the velocity of the tether relative to the given velocity $v = (v_1, v_2)$ of the blood flow near the leukocyte, where we always assume $v = O(|\mathcal{U}|)$, for $|\mathcal{U}| \to 0$. The superscript $\perp$ indicates rotation by $\pi/2$.

Two different situations will be considered:

1) The tether is anchored to the vessel wall. In this case the boundary conditions

$$T(0,t) = T_0\,, \qquad T(\kappa(t),t) = T_1(t)\,, \qquad \partial_s^2 T(0,t) = \partial_s^2 T(\kappa,t) = 0\,,$$

are used, where the time dependence of T_1 is caused by the movement of the leukocyte.

2) The end of the tether is free. Now the boundary conditions

$$\zeta\kappa\partial_s T(0,t) - \mu\partial_s^3 T(0,t) = 0\,,\ T(\kappa(t),t) = T_1(t)\,,\ \partial_s^2 T(0,t) = \partial_s^2 T(\kappa,t) = 0\,,$$

apply. The problem is completed by prescribing initial conditions

$$T(s,0) = T_I(s)\,,$$

and we recall the condition

$$\kappa = \int_0^{\kappa} |\partial_s T|\ ds\,.$$

Well posedness of this moving boundary problem seems highly nontrivial.

3. Simplifications

Before we start analyzing the above problem, we will make some simplifications and approximations in order to end up with a special case of the original model.

The first major assumption will be, that the whole process is observed as *quasi-stationary*. This approximation requires that the characteristic velocity of the object is much smaller than the propagation velocity of information relating to this object. Biologically, this is quite reasonable in our case, since the motion of the neutrophil is assumed to be much slower than the dynamics of the tether. Time-dependence therefore is assumed to be negligible, which leads to setting all time derivatives equal to zero. Also the given velocity field, v, will not depend on t. Furthermore, under this assumptions it makes no sense to investigate the process after tether breaking. Hence, our tether will be fixed at one end at the neutrophil and at the other end on the vessel wall and time-independent given boundary conditions will be used.

Furthermore, we will have a closer look at the friction term in our now quasi-stationary problem. The friction-force in normal direction is much stronger than the force in the tangential direction. Therefore, $\gamma^{\|}$ is assumed to be that small, that the corresponding term in the differential equations does not contribute significantly and hence, will be ignored completely. Thus, another simplification will be setting $\gamma^{\|} = 0$.

At last, we will switch the roles of the endpoints of the tether such that the

parameter interval is orientated the same way as the x-axis. Since we now assume that κ does not change in time, it does not matter weather $s = \kappa$ corresponds to the endpoint of the tether at the cell or to the endpoint anchored at the vessel wall. For reasons of simplification we therefore use the convention that at $s = 0$ the tether originates from the leukocyte and at $s = \kappa$ the tether is anchored at the blood vessel wall.
The partial differential equations (1) simplify to ordinary differential equations, the arc-length, κ, is not time-dependent anymore and the problem now reads

$$\begin{aligned} -\mu T^{(4)} + \zeta\kappa T'' + \frac{\gamma^{\perp}}{|T'|^2}(T'^{\perp} \cdot v(T))\, T'^{\perp} = 0, \text{ for } s \in (0,\kappa), \\ \int_0^{\kappa} |T'|\, ds = \kappa, \end{aligned} \tag{2}$$

where $T'^{\perp}(s) = \begin{pmatrix} -T_2'(s) \\ T_1'(s) \end{pmatrix}$ again denotes the unit normal vector of T and the boundary conditions are given by

$$\begin{aligned} &T'' = 0, \text{ for } s = 0, \kappa \\ &T(0) = T_0 \text{ and } T(\kappa) = T_1 \text{ given.} \end{aligned} \tag{3}$$

3.1. **The Tether as Graph of a Function.** The next assumption will concern the curve describing the tether itself. We assume that the displacement of the tether under the blood flow is that little, that the curve can always be expressed as graph of some function denoted by u. Here we want to recall that we assume for the velocity of the blood flow near the cell $v = O(|\mathcal{U}|)$. Then of course, this assumption is only reasonable in a physical way, if $|\mathcal{U}|$, the speed of the blood flow, is suitable small. As we will see later on, an adequate small speed is absolutely necessary for our analysis to work.
In other words, we assume that there exists some function $u : [x_0, x_1] \mapsto \mathbb{R}$ for some $x_0, x_1 > 0$, such that the curve can be parametrized by

$$T : [x_0, x_1] \mapsto \mathbb{R}^2, \quad T(x) = \begin{pmatrix} x \\ u(x) \end{pmatrix}.$$

This will help us to reduce the problem (2) from two dimensions to only one, given by one differential equation for u.
We further introduce $\bar{u} : [x_0, x_1] \mapsto \mathbb{R}$, which describes the interpolation between the endpoints of the tether, and its length, κ_0. If the boundary conditions are given by $T(x_0) = \begin{pmatrix} x_0 \\ u_0 \end{pmatrix}$ and $T(x_1) = \begin{pmatrix} x_1 \\ 0 \end{pmatrix}$, then

$$\bar{u}(x) = \frac{u_0}{x_1 - x_0}(x_1 - x)$$

and

$$\kappa_0 = \sqrt{(x_1 - x_0)^2 + u_0^2}.$$

Regarding our assumption, u always has to remain in a small neighborhood around $\bar{u}$. If we write $u(x) = \bar{u}(x) + w(x)$, $\forall x \in [x_0, x_1]$, this allows us to

reduce the problem to investigating the dynamics of the perturbation w, as we will use several times later on. The assumption that $|\mathcal{U}|$ is that small that there is only very little displacement from the interpolation also implies that the slope of u is very close to the one of $\bar{u}$ and therefore, w' is small.

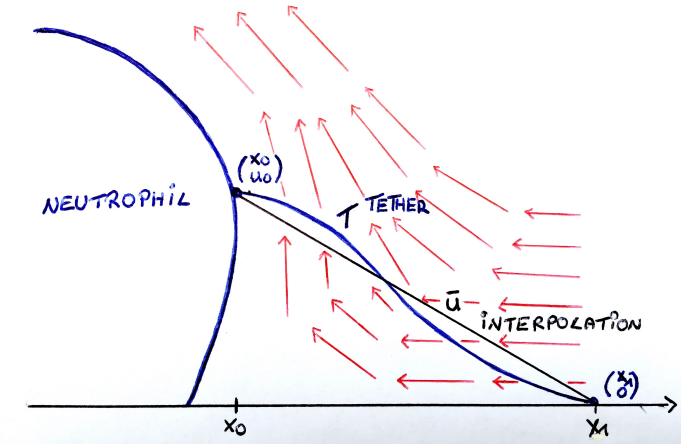

FIGURE 6. Sketch of the 2D-model with interpolation $\bar{u}$

Working with such a comfortable way to parametrize the curve goes along with further approximations which will not always be consistent. Since neither x is the parameter by which we differentiate nor $x_1 - x_0$ is the actual length of the curve, we have to find a suitable parameter transformation. Considering a velocity field with small $|\mathcal{U}|$ gives us from the first differential equation in (2) after neglecting the friction term

$$T_1(s) \sim \varphi(s) := \frac{x_1 - x_0}{\kappa} s + x_0,$$

with $\varphi : [0, \kappa] \mapsto [x_0, x_1]$ defining a regular parameter transformation from $[0, \kappa]$ to $[x_0, x_1]$. Therefore, T will be written as

$$T(x) = \begin{pmatrix} x \\ u(x) \end{pmatrix} = \begin{pmatrix} \varphi(s) \\ u(\varphi(s)) \end{pmatrix} \sim T(s).$$

Here, we want to mention that only doing a linear approximation of the first component of T, while still considering friction in the second one, is not a consistent approximation.
By using the chain rule, one can express the derivatives with respect to s as ones with respect to x by $\frac{dT}{ds} = \frac{dT}{dx}\frac{x_1 - x_0}{\kappa}$. In the formula for κ we use our above assumption, that the slope of u can be approximated by the one of $\bar{u}$, for the first time. We get

$$\kappa = \int_{x_0}^{x_1} \sqrt{1 + u'^2(x)}\, dx \sim \int_{x_0}^{x_1} \sqrt{1 + \bar{u}'^2(x)}\, dx = \kappa_0,$$

and the derivatives can be approximated by $\frac{dT}{ds} \sim \frac{x_1 - x_0}{\kappa_0}\frac{dT}{dx}$. Keeping in mind that

$$\frac{T'^{\perp}(x)}{|T'(x)|} = \frac{1}{\sqrt{1 + u'^2(x)}} \begin{pmatrix} -u'(x) \\ 1 \end{pmatrix}$$

is the unit normal vector at $x \in [x_0, x_1]$ in the last term of the equation (2), we can rewrite our problem. The simplified and now only one-dimensional differential equation in our problem reads

$$-\mu \left(\frac{x_1 - x_0}{\kappa_0}\right)^4 u^{(4)} + \zeta\kappa \left(\frac{x_1 - x_0}{\kappa_0}\right)^2 u'' + \gamma^{\perp} \frac{v_2 - v_1 u'}{1 + u'^2} = 0. \tag{4}$$

The curvature κ remains as the last open question concerning these approximations. In order to maintain the property that stretching the tether in longitudinal direction is proportional to the actual length of it, we won't use the constant length κ_0 of the interpolation as approximation.
Also in this case we will perform a linear approximation where we assume the slope of u being very close to the one of $\bar{u}$. By Taylor-expansion up to order u'^2 we get for the arc-length:

$$\begin{aligned}
\int_{x_0}^{x_1} \sqrt{1 + u'^2}\, dx &= \int_{x_0}^{x_1} \sqrt{1 + \left(w' - \frac{u_0}{x_1 - x_0}\right)^2}\, dx \\
&= \frac{\kappa_0}{x_1 - x_0} \int_{x_0}^{x_1} \sqrt{1 - 2w' \frac{u_0(x_1 - x_0)}{\kappa_0^2} + \frac{w'^2 (x_0 - x_1)^2}{\kappa_0^2}}\, dx \\
&\sim \frac{\kappa_0}{x_1 - x_0} \int_{x_0}^{x_1} \left[1 - w' \frac{u_0(x_1 - x_0)}{\kappa_0^2} + \frac{w'^2 (x_0 - x_1)^2}{2\kappa_0^2} - \frac{w'^2 (x_1 - x_0)^2 u_0^2}{2\kappa_0^4}\right] dx \\
&= \kappa_0 + \frac{(x_1 - x_0)^3}{2\kappa_0^3} \int_{x_0}^{x_1} w'^2\, dx,
\end{aligned}$$

where in the last equality we used that w vanishes at the boundary. After substituting $w = u - \bar{u}$ and several calculations, we get

$$\begin{aligned}
&\int_{x_0}^{x_1} \sqrt{1 + u'^2}\, dx \sim \\
&\frac{u_0^4 + (x_1 - x_0)^4 + \frac{3}{2} u_0^2 (x_1 - x_0)^2}{\kappa_0^3} + \frac{(x_1 - x_0)^3}{2\kappa_0^3} \int_{x_0}^{x_1} u'^2\, dx =: \kappa[u].
\end{aligned} \tag{5}$$

For simplicity let us denote

$$\tilde{c} := \frac{u_0^4 + (x_1 - x_0)^4 + \frac{3}{2} u_0^2 (x_1 - x_0)^2}{\kappa_0^3} \tag{6}$$

and therefore,

$$\kappa[u] = \tilde{c} + \frac{(x_1 - x_0)^3}{\kappa_0^3} \int_{x_0}^{x_1} \frac{u'^2}{2}\, dx.$$

Our now fully simplified model is given by

$$\begin{aligned}
&-\mu \left(\frac{x_1 - x_0}{\kappa_0}\right)^4 u^{(4)} + \zeta\kappa[u] \left(\frac{x_1 - x_0}{\kappa_0}\right)^2 u'' + \gamma^{\perp} \frac{v_2 - v_1 u'}{1 + u'^2} = 0, \\
&\qquad \text{for } \; x \in (x_0, x_1), \\
&\kappa[u] = \tilde{c} + \frac{(x_1 - x_0)^3}{\kappa_0^3} \int_{x_0}^{x_1} \frac{u'^2}{2}\, dx, \\
&u(x_0) = u_0, \; u(x_1) = 0, \\
&u''(x_0) = u''(x_1) = 0.
\end{aligned} \tag{7}$$

3.2. **The Blood Flow as Two-Dimensional Potential Flow.** With this simplifications we achieved a workable model, but there still is one magnitude not described clearly. The last open question is how to model the two-dimensional quasi-stationary blood flow v around the cell. We assumed the blood streaming as a laminar flow from the right to the left with velocity $\hat{v} := \begin{pmatrix} \mathcal{U} \\ 0 \end{pmatrix}, \mathcal{U} < 0$. But this velocity cannot be used near the neutrophil where we would need it, since the streamlines are diverted by the cell. In this work, we will simulate the bloodstream around the cell by calculating velocity fields, which describe a flow between two lines enclosing a specific angle. One line will be the x-axis simulating the vessel wall, the other one will serve as modell for the cell. The idea and procedure was taken from [6].

In order to determine such a velocity field of the bloodstream, we assume that the flow is a *potential flow* and hence, can be written as the gradient of some scalar function, the so-called *velocity potential*. If we denote this velocity potential by Φ, we get $\hat{v} = \nabla\Phi$. Furthermore, the blood flow is an *incompressible flow*, which is equivalent to require that the velocity field $\hat{v}$ is divergence free, i.e. $\nabla \cdot \hat{v} = 0$. This again implies that the potential Φ has to satisfy the *Laplace equation*, $\Delta\Phi = 0$ and hence, is a *harmonic function*. We now take use of the fact, that our blood flow is two-dimensional and interpret $\mathbb{R}^2$ as complex plane. In this case, our potential flow occurs in the upper half-plane $\mathbb{H} := \{x + iy \mid y > 0;\ x, y \in \mathbb{R}\}$ and we will investigate it further by using a holomorphic mapping. Let us denote $z := x + iy$, then we define the *complex velocity potential*

$$F(z) := \Phi(x, y) + i\Psi(x, y), \quad \forall z \in \mathbb{C},$$

where the real valued functions Φ and Ψ are the real and imaginary part of F. Since we assume F to be holomorphic, Φ and Ψ have to satisfy the *Cauchy-Riemann equations*,

$$\frac{\partial\Phi}{\partial x} = \frac{\partial\Psi}{\partial y}, \quad \frac{\partial\Phi}{\partial y} = -\frac{\partial\Psi}{\partial x}.$$

One gets by further differentiation that both Φ and Ψ have to be harmonic, i.e. $\Delta\Phi = 0$ and $\Delta\Psi = 0$. Therefore, our velocity potential of our flow can be interpreted as the real part of a holomorphic function.

In our case, we have $\hat{v}(x, y) = \nabla\Phi(x, y) = \begin{pmatrix} \mathcal{U} \\ 0 \end{pmatrix}, \forall (x, y) \in \mathbb{H}$ and by using the Cauchy-Riemann equations, we get

$$\Phi(x, y) = \mathcal{U}x, \quad \Psi(x, y) = \mathcal{U}y,$$

and therefore the complex velocity potential reads

$$F(z) = \mathcal{U}z, \quad z \in \mathbb{H}.$$

We will now use the fact, that a harmonic function under a transformation by a conformal map remains harmonic. This means that our Φ remains harmonic after transforming the complex upper half-plane via an angle- and orientation-preserving map. We will give two attempts of simulating the blood flow around a neutrophil. Firstly, the conformal transformation of $\mathcal{H}$ is given by the square-root, which will give us the flow between the positive

parts of the x- and the y-axis (enclosing an angle of 90°). Secondly, a more realistic simulation is tried to be achieved by using the fifth-root in order to get a velocity field of a flow between the positive parts of the x-axis and a line with which it encloses an angle of 36°.

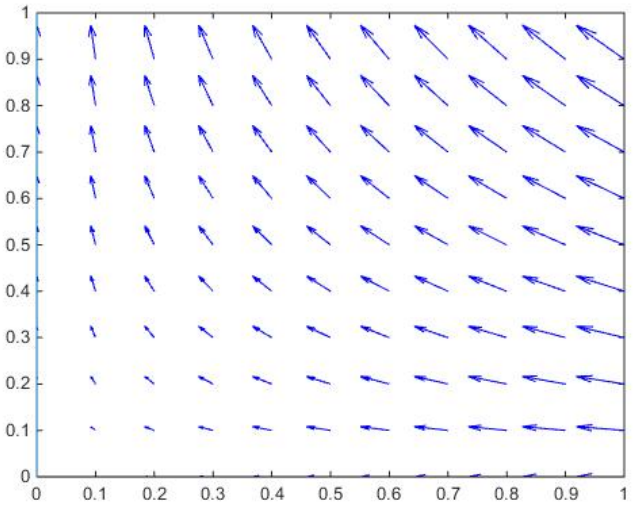

FIGURE 7. Velocity field with speed $\mathcal{U} = -1$ after taking the square-root of the upper half-plane

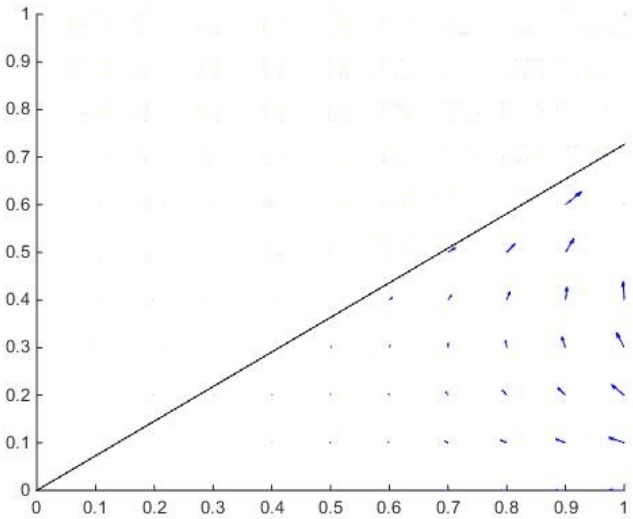

FIGURE 8. Velocity field with speed $\mathcal{U} = -1$ after taking the fifth-root of the upper half-plane

3.2.1. *Square-Root.* Let us denote by $\xi := \sqrt{z}$, $\xi := a + ib$, the variable after coordinate transformation and by $W(\xi) := F(\xi^2)$, the complex velocity potential in the transformed domain. We get

$$W(\xi) = \mathcal{U}\xi^2 = \mathcal{U}(a^2 - b^2 + i2ab).$$

Hence, the potential velocity after transformation is given by $\tilde{\Phi}(a,b) = \mathcal{U}(a^2 - b^2)$, for $a, b > 0$ and therefore, one gets for the velocity field

$$v_{sqrt}(a,b) := 2\mathcal{U}\begin{pmatrix} a \\ -b \end{pmatrix}, \text{ for } a, b > 0.$$

Our domain therefore is the first quadrant, where the a-axis can be seen as the vessel wall, while the b-axis serves as replacement for the neutrophil.

3.2.2. *Fifth-Root.* Using the same notation as before, we set $\xi := \sqrt[5]{z}$ and $W(\xi) := F(\xi^5)$. Calculating the complex velocity potential gives

$$W(\xi) = \mathcal{U}(a^5 - 10a^3b^2 + 5ab^4 + i(5a^4b - 10a^2b^3 + b^5)).$$

From this we conclude that the new potential velocity reads $\tilde{\Phi}(a,b) = \mathcal{U}(a^5 - 10a^3b^2 + 5ab^4)$ and the velocity field of the flow in the transformed domain is given by

$$v_{ftrt}(a,b) := \mathcal{U}\begin{pmatrix} 5a^4 - 30a^2b^2 + 5b^4 \\ -20a^3b + 20ab^3 \end{pmatrix}.$$

We are interested in the domain given by $\{a, b \in \mathbb{R}^3 \,:\, a > 0, b > 0 \text{ and } b < a\sqrt{5 - \sqrt{20}}\}$. Here, the line given by $b = a\sqrt{5 - \sqrt{20}}$ serves as replacement for the cell.

Part 3. Theoretical Analysis

The main goal of this chapter is to investigate the system (7) and prove existence and uniqueness of a solution. Our problem can be classified as one-dimensional boundary value problem and is analyzed by using results and methods from functional analysis. More details to the theoretical background and methods used can be found, for example, in [1].

Since, apart from the speed of the blood flow $\mathcal{U}$, which is contained in the formular of v, none of the constants are important for the analysis of (7), we reformulate the system using the notation

$$a := \mu \left(\frac{x_1 - x_0}{\kappa_0} \right)^4, \quad b := \zeta \left(\frac{x_1 - x_0}{\kappa_0} \right)^2.$$

Here, it is important to note that $b\kappa[u]$ is always positive. Furthermore, we write $\tilde{p} = \tilde{p}(x, u(x), u'(x)) = v_2(x, u(x)) - v_1(x, u(x))u'(x)$ for a polynomial in x, u and u'. In our case, we have

$$\tilde{p}(x, u(x), u'(x)) = p_{sqrt}(x, u(x), u'(x)) = u(x) + xu'(x), \tag{8}$$

if we consider our problem (7) with the velocity field of the blood flow given by $v = v_{sqrt}$ and

$$\begin{aligned} &\tilde{p}(x, u(x), u'(x)) = p_{ftrt}(x, u(x), u'(x)) \\ &\quad = 5x^4u'(x) + 5u^4(x)u'(x) - 30x^2u^2(x)u'(x) + 20x^3u(x) - 20xu^3(x), \end{aligned} \tag{9}$$

if we use $v = v_{ftrt}$ as velocity field. In order to be able to work with homogeneous boundary conditions, we again use the fact that $u = \bar{u} + w$, with w being the perturbation from the interpolation $\bar{u}$. Keeping in mind that

$$u'(x) = \bar{u}' + w'(x) = -\frac{u_0}{x_1 - x_0} + w'(x)$$

and that

$$p(x, w(x), w'(x)) := \tilde{p}(x, \bar{u}(x) + w(x), \bar{u}' + w'(x))$$

defines a polynomial in x, w and w', we reformulate our problem further such that now w is our unknown. Since $u(x_0) = \bar{u}(x_0) = u_0$ and $u(x_1) = \bar{u}(x_1) = 0$ we get the desired homogeneous boundary conditions $w(x_0) = w(x_1) = 0$. The formula for the curvature is then given by

$$\kappa[\bar{u} + w] = \tilde{c} + \frac{(x_1 - x_0)^3}{\kappa_0^3} \int_{x_0}^{x_1} \frac{1}{2} \left(\frac{-u_0}{x_1 - x_0} + w' \right)^2 \, dx. \tag{10}$$

The problem we investigate now reads

$$\begin{aligned} &-aw^{(4)}(x) + b\kappa[\bar{u} + w]w''(x) = 2\mathcal{U}\gamma^{\perp} \frac{p(x, w(x), w'(x))}{1 + (\bar{u}' + w'(x))^2} \quad \text{in } (x_0, x_1), \\ &w(x_0) = w(x_1) = 0, \\ &w''(x_0) = w''(x_1) = 0, \\ &\text{and} \quad \kappa[\bar{u} + w] = \tilde{c} + \frac{(x_1 - x_0)^3}{\kappa_0^3} \int_{x_0}^{x_1} \frac{1}{2} \left(\frac{-u_0}{x_1 - x_0} + w' \right)^2 \, dx. \end{aligned} \tag{11}$$

In order to prove existence and uniqueness of (11), we will do a fixed-point iteration. For given function w_n, in each step the solution w_{n+1} of the system

(12)
$$\begin{aligned} &-aw_{n+1}^{(4)}(x) + b\kappa[\bar{u}+w_n]w_{n+1}''(x) = 2\mathcal{U}\gamma^{\perp}\frac{p(x,w_n(x),w_n'(x))}{1+(\bar{u}'+w_n'(x))^2} \quad \text{in } (x_0,x_1),\\ &w_{n+1}(x_0) = w_{n+1}(x_1) = 0,\\ &w_{n+1}''(x_0) = w_{n+1}''(x_1) = 0, \end{aligned}$$

is calculated. The resulting sequence $\{w_n\}_{n\geq 1}$ is convergent and its limit then is the solution of the original problem (11).
Therefore, the first aim is to prove existence and uniqueness of a solution of the linear problem (12). This we will do by applying the *Lax-Milgram theorem*. Afterward, convergence of the sequence is shown using *Banach's fixed-point theorem*. Both results are stated in [1].

1. Analysis of the Linear Problem

We will work on the space $H_\partial^2 := \{w \in H^2(x_0,x_1) \mid w(x_0) = w(x_1) = 0\}$ equipped with the H^2-norm.
We first formulate the linear problem (12) for a given continuously differentiable function. Let $\tilde{w} \in H_\partial^2$, then of course the curvature $\kappa := \kappa[\bar{u}+\tilde{w}]$ is constant and we define

$$f(x) := 2\gamma^{\perp}\frac{p(x,\tilde{w}(x),\tilde{w}'(x))}{1+(\bar{u}'+\tilde{w}'(x))^2}, \quad x \in [x_0,x_1].$$

Since $\tilde{w}$ is assumed to be in H_∂^2, we can use a *Sobolev-embedding* theorem (in one dimension) and conclude $\tilde{w} \in C^1[x_0,x_1]$. More general information to *Sobolev inequalities* can, again, be found in [1]. This implies that f is continuous, hence bounded on $[x_0,x_1]$ and therefore we get a function in $L^2[x_0,x_1]$ on the right-hand-side. The problem to investigate in each iteration step now reads

$$\begin{aligned} -aw^{(4)} + b\kappa w'' &= \mathcal{U}f \quad \text{in } (x_0,x_1),\\ w(x_0) = w(x_1) &= 0,\\ w''(x_0) = w''(x_1) &= 0. \end{aligned} \tag{13}$$

1.1. Existence of a weak solution.

After multiplying the differential equation in (13) with a testfunction $\varphi \in H_\partial^2$ and integrating by parts while ignoring the resulting boundary terms, we end up with

$$a\int_{x_0}^{x_1}\varphi''w''\,dx + b\kappa + \int_{x_0}^{x_1}\varphi'w'\,dx = -\mathcal{U}\int_{x_0}^{x_1}\varphi f\,dx.$$

Lets define the *bilinear form*

$$A : H_\partial^2 \times H_\partial^2 \to \mathbb{R}, \quad A(\varphi,w) := a\int_{x_0}^{x_1}\varphi''w''\,dx + b\kappa\int_{x_0}^{x_1}\varphi'w'\,dx,$$

and the *linear functional*

$$F : H_\partial^2 \to \mathbb{R}, \quad F(\varphi) := -\mathcal{U}\int_{x_0}^{x_1}\varphi f\,dx.$$

Since $f \in L^2(x_0, x_1)$, one can see easily by the *Cauchy-Schwarz inequality* that

$$\begin{aligned} |F(\varphi)| &\leq |\mathcal{U}| \|\varphi f\|_{L^1(x_0,x_1)} \\ &\leq |\mathcal{U}| \|\varphi\|_{L^2(x_0,x_1)} \|f\|_{L^2(x_0,x_1)}, \end{aligned}$$

and therefore F is bounded and can be seen as an element of $H_\partial^{2'}$, the dual space of H_∂^2. The *weak formulation* of our problem is finding a solution $w \in H_\partial^2$, such that $A(\varphi, w) = F(\varphi)$, $\forall \varphi \in H_\partial^2$. To prove the existence and uniqueness of such a weak solution, we will use the Lax-Milgram theorem. Therefore, we fist have to show that A is a *continuous* and *coercive* bilinear form.

1.1.1. *Continuity.* Let $\varphi, w \in H_\partial^2$, then

$$\begin{aligned} |A(\varphi, w)| &\leq a\|\varphi'' w''\|_{L^1(x_0,x_1)} + b\kappa \|\varphi' w'\|_{L^1(x_0,x_1)} \\ &\leq a\|\varphi''\|_{L^2(x_0,x_1)} \|w''\|_{L^2(x_0,x_1)} + b\kappa \|\varphi'\|_{L^2(x_0,x_1)} \|w'\|_{L^2(x_0,x_1)} \\ &\leq (a + b\kappa) \|\varphi\|_{H^2(x_0,x_1)} \|w\|_{H^2(x_0,x_1)}, \end{aligned}$$

where in the second inequality we again used Cauchy-Schwarz and in the last one, we simply used the definition of the H^2-norm.

1.1.2. *Coercivity.* In order to show the coercivity of A, we use *Poincarè's inequality*. We will state a special version in one dimension concerning L^2, the general theorem can be found in [1].

Lemma 1 (Poincarè's inequality)**.** *Let I be a bounded open interval, then there exists some constant λ_p (depending on I), such that*

$$\|w\|_{L^2(I)} \leq \lambda_p \|w'\|_{L^2(I)}, \quad \forall w \in H_0^1(I).$$

Let $w \in H_\partial^2 \subset H_0^1(x_0, x_1)$, then we can use the above lemma and the following estimates

$$\begin{aligned} A(w, w) &= a\|w''\|^2_{L^2(x_0,x_1)} + b\kappa \|w'\|^2_{L^2(x_0,x_1)} \\ &= a\|w''\|^2_{L^2(x_0,x_1)} + \frac{b\kappa}{2}\|w'\|^2_{L^2(x_0,x_1)} + \frac{b\kappa}{2}\|w'\|^2_{L^2(x_0,x_1)} \\ &\geq a\|w''\|^2_{L^2(x_0,x_1)} + \frac{b\kappa}{2}\|w'\|^2_{L^2(x_0,x_1)} + \frac{1}{\lambda_p}\frac{b\kappa}{2}\|w\|^2_{L^2(x_0,x_1)} \\ &\geq \min\left\{a, \frac{b\kappa}{2}, \frac{b\kappa}{2\lambda_p}\right\} \|w\|^2_{H^2(x_0,x_1)} \end{aligned}$$

give us the coercivity of A.

Now, we can apply the Lax-Milgram theorem, which gives us the existence of a unique weak solution, i.e.

$$\exists! w \in H_\partial^2(x_0, x_1) \text{ such that } A(w, \varphi) = F(\varphi), \quad \forall \varphi \in H_\partial^2(x_0, x_1). \tag{14}$$

1.2. **Regularity.** Up to this point, it is not clear whether the weak solution $w \in H^2_\partial$ also solves the original problem (13).
From Lax-Milgram we get the estimate

$$\begin{aligned} \|w\|_{H^2(x_0,x_1)} &\leq k\|F\|_{H^{2'}_\partial} \\ &\leq k|\mathcal{U}|\|f\|_{L^2(x_0,x_1)}, \end{aligned} \tag{15}$$

with k being the inverse of the coercivity constant of A and hence we see that $w \in H^2(x_0, x_1)$. Due to the fact that we are only in one dimension and applying a Sobolev-embedding theorem assures us that w can be interpreted as an element in $C^1[x_0, x_1]$, which we already used once above. Therefore, we can now say that our solution w fulfills $w \in C^1[x_0, x_1]$ and $w(x_0) = w(x_1) = 0$. But to solve (13) more smoothness is needed.
After integration by parts and only considering testfunctions $\varphi \in C_0^\infty(x_0, x_1)$, we get from (14) that

$$w^{(4)} = \frac{1}{a}[b\kappa w'' - \mathcal{U}f], \tag{16}$$

in the sense of distributions. Since we have $w \in H^2(x_0, x_1)$ and assumed $f \in L^2(x_0, x_1)$, we see from the above equation that $w^{(4)} \in L^2(x_0, x_1)$. In order to control w''', we use the following version of the *Gagliardo-Nirenberg interpolation inequality*, which can be found in [5].

Theorem 2 (Gagliardo-Nirenberg interpolation inequality)**.** *Let $\Omega \in \mathbb{R}^n$ be a bounded Lipschitz domain, and $u : \Omega \to \mathbb{R}$. Let $1 \leq p, q, r \leq \infty$ and $m, j \in \mathbb{N}$ be fixed. If*

$$\frac{1}{p} = \frac{j}{n} + \left(\frac{1}{r} - \frac{m}{n}\right)\alpha + \frac{1-\alpha}{q},$$

$$\frac{j}{m} \leq \alpha \leq 1$$

and $u \in L^q(\Omega)$, $\nabla^m u \in L^r(\Omega)$, then

$$\nabla^j u \in L^p(\Omega).$$

Furthermore, $\exists C_1, C_2$ such that the following inequality

$$\|\nabla^j u\|_{L^p(\Omega)} \leq C_1\|\nabla^m u\|^\alpha_{L^r(\Omega)}\|u\|^{1-\alpha}_{L^q(\Omega)} + C_2\|u\|_{L^s(\Omega)},$$

holds for $s > 0$ arbitrary. The constants are only depending on n, m, j, p, q, r, α and s.

In our case we use that $w, w^{(4)} \in L^2(x_0, x_1)$ to control w'''. Regarding the above theorem this means $p = q = r = 2$ and $j = 3$, $m = 4$, which gives us $\alpha = \frac{3}{4}$. The interpolation inequality

$$\|w'''\|_{L^2(x_0,x_1)} \leq C_1\|w^{(4)}\|^{\frac{3}{4}}_{L^2(x_0,x_1)}\|w\|^{\frac{1}{4}}_{L^2(x_0,x_1)} + C_2\|w\|_{L^s(x_0,x_1)},$$

for suitable constants C_1, C_2 and for $s = 2$ assures us

$$w''' \in L^2(x_0, x_1).$$

Therefore, we can conclude

$$w \in H^4(x_0, x_1).$$

Again after applying Sobolev's embedding theorem this yields $w \in C^3[x_0, x_1]$, which is still not enough to solve (13). But since we now know that w'' is continuous (even in $C^1[x_0, x_1]$), we get that both f and f' are also continuous, hence bounded on $[x_0, x_1]$. This implies that f and its derivate are L^2-functions, which gives us $f \in H^1(x_0, x_1)$. Having in mind that $w \in H^4(x_0, x_1)$ we can conclude from (16) that $w^{(4)} \in H^1(x_0, x_1)$ and therefore Gagliardo-Nirenberg gives us $w \in H^5(x_0, x_1)$. With Sobolev's embedding theorem we have that $w \in C^4(x_0, x_1)$, which assures that the solution is smooth enough to fulfill the differential equation in (13).

In order to be sure that our smooth w also is a solution of the whole problem (13), we have to show that it actually solves the differential equation and it also fulfills the freely rotating boundary conditions

$$w''(x_0) = w''(x_1) = 0.$$

For this, let us again consider the weak formulation of the problem:

$$\begin{aligned} &A(\varphi, w) - F(\varphi) = 0 \\ &\Leftrightarrow \\ &a \int_{x_0}^{x_1} \varphi'' w'' \, dx + b\kappa \int_{x_0}^{x_1} \varphi' w' \, dx + \mathcal{U} \int_{x_0}^{x_1} \varphi f \, dx = 0, \end{aligned}$$

for some $\varphi \in H^2_\partial$. Since we now know that w is smooth, we can integrate by parts such that only w occurs with derivatives:

$$\begin{aligned} &a \int_{x_0}^{x_1} \varphi w^{(4)} \, dx + a \, (\varphi' w'')\big|_{x_0}^{x_1} - a \, (\varphi w''')\big|_{x_0}^{x_1} \\ &- b\kappa \int_{x_0}^{x_1} \varphi w'' \, dx + b\kappa \, (\varphi w')\big|_{x_0}^{x_1} + \mathcal{U} \int_{x_0}^{x_1} \varphi f \, dx = 0. \end{aligned}$$

The testfunction $\varphi \in H^2_\partial$ vanishes at the boundary, which implies that the third and the fifth term in the above equation are equal to zero. We get that

$$a \int_{x_0}^{x_1} \varphi w^{(4)} \, dx + a \, (\varphi' w'')\big|_{x_0}^{x_1} - b\kappa \int_{x_0}^{x_1} \varphi w'' \, dx + \mathcal{U} \int_{x_0}^{x_1} \varphi f \, dx = 0. \tag{17}$$

Let us now only consider testfunctions whose derivatives have compact support, i.e. $\varphi \in H^2_\partial$ such that $\varphi'(x_0) = \varphi'(x_1) = 0$. Then also the last boundary term vanishes and

$$a \int_{x_0}^{x_1} \varphi w^{(4)} \, dx - b\kappa \int_{x_0}^{x_1} \varphi w'' \, dx + \mathcal{U} \int_{x_0}^{x_1} \varphi f \, dx = 0,$$

has to hold $\forall \varphi \in \{H^2_\partial \,|\, \varphi'(x_0) = \varphi'(x_1) = 0\}$. From this we can conclude that w fulfills the differential equation in (13) for $x \in (x_0, x_1)$.
Again considering (17), we now know that

$$a \, (\varphi' w'')\big|_{x_0}^{x_1} = 0.$$

Firstly, we restrict ourselves to $\varphi \in H^2_\partial$ with $\varphi'(x_0) = 1$ and $\varphi'(x_1) = 0$ and therfore conclude $w''(x_0) = 0$. Secondly, we only take $\varphi \in H^2_\partial$ with $\varphi'(x_0) = 0$ and $\varphi'(x_1) = 1$ and get $w''(x_1) = 0$.

With this, we finally proved that the weak solution w is also a classical solution to the linear problem (13).

2. Convergence of the Fixed-Point Iteration

In this section, we will prove convergence of the fixed-point iteration given by solving (12) in each step. We want to apply Banach's fixed-point theorem on the space

$$\mathcal{S} := \left\{ v \in H^2_\partial(x_0, x_1) \mid \|v\|_{H^2(x_0,x_1)} \leq M \right\},$$

for some fixed constant $M > 0$ and on the, as we proved in the last section, well defined mapping G given by

$$\begin{aligned} &G: \ H^2(x_0,x_1) \to H^2(x_0,x_1), \quad \tilde{w} \overset{G}{\mapsto} w \text{ by solving:} \\ &-aw^{(4)} + (b\kappa[\bar{u}+\tilde{w}]+c)w'' = \mathcal{U} f[\tilde{w}] \quad \text{in } (x_0,x_1), \\ &w(x_0) = w(x_1) = 0, \\ &w''(x_0) = w''(x_1) = 0. \end{aligned} \tag{18}$$

Again with the already familiar notation

$$f[\tilde{w}](x) = \frac{p(x,\tilde{w},\tilde{w}')}{1+(\bar{u}'+\tilde{w}')^2}, \quad x \in [x_0,x_1].$$

Here, the subscript at the right-hand-side emphasizes that it depends on the input function $\tilde{w}$. We have to prove that G maps $\mathcal{S}$ into itself and that G is a contraction on $\mathcal{S}$. Now it is very important that we assumed our model to be reasonable only with a suitable small blood flow speed $\mathcal{U}$.

In order to see that G maps $\mathcal{S}$ into itself, we use the estimate (15) we get from the Lax-Milgram theorem. Let again be $\tilde{w} \in \mathcal{S}$ some input and $w := G(\tilde{w})$. Then we have

$$\begin{aligned} \|w\|_{H^2(x_0,x_1)} &\leq k|\mathcal{U}| \|f[\tilde{w}]\|_{L^2(x_0,x_1)} \\ &= k|\mathcal{U}| \left(\int_{x_0}^{x_1} \frac{p(x,\tilde{w}(x),\tilde{w}'(x))^2}{(1+(\bar{u}'+\tilde{w}'(x))^2)^2} \, dx \right)^{\frac{1}{2}} \\ &\leq k|\mathcal{U}| \left(\int_{x_0}^{x_1} p(x,\tilde{w}(x),\tilde{w}'(x))^2 \, dx \right)^{\frac{1}{2}} \\ &\leq k|\mathcal{U}| \sqrt{x_1-x_0} \|p(.,\tilde{w}(.),\tilde{w}'(.))\|_{L^\infty(x_0,x_1)}. \end{aligned} \tag{19}$$

Since $\tilde{w} \in C^1(x_0,x_1)$ due to Sobolev's embedding, we have that both $\tilde{w}$ and $\tilde{w}'$ are bounded on $[x_0,x_1]$ and therefore we can estimate p with a monotone increasing function h of the L^∞-norms of $\tilde{w}$ and $\tilde{w}'$. Afterward we can use the Sobolev-embedding inequality to end up with the H^2-norm of $\tilde{w}$.

$$\begin{aligned} \|w\|_{H^2(x_0,x_1)} &\leq |\mathcal{U}| h(\|\tilde{w}\|_{L^\infty(x_0,x_1)} + \|\tilde{w}'\|_{L^\infty(x_0,x_1)}) \\ &= |\mathcal{U}| h(\|\tilde{w}\|_{C^1([x_0,x_1])}) \\ &\leq |\mathcal{U}| h(\|C\tilde{w}\|_{H^2(x_0,x_1)}) \\ &\leq |\mathcal{U}| h(CM) \\ &\leq M \end{aligned} \tag{20}$$

for $\mathcal{U}$ suitable small and therefore, w also lies in $\mathcal{S}$.

We now want to prove that G is a contraction. Let $\tilde{w}_1, \tilde{w}_2 \in \mathcal{S}$, $w_1 := G(\tilde{w}_1)$, $w_2 := G(\tilde{w}_2)$ and $u_1 := \bar{u} + \tilde{w}_1$, $u_2 := \bar{u} + \tilde{w}_2$. We now consider the problem (21) for both $\tilde{w}_1$, w_1 and $\tilde{w}_2$, w_2 and subtract the second differential equation from the first one. By using the notation $v := w_1 - w_2$ and $f_j := f[\tilde{w}_j]$, $j \in \{1, 2\}$, we get

$$-av^{(4)} + b(\kappa[u_1]w_1'' - \kappa[u_2]w_2'') = \mathcal{U}(f_1 - f_2).$$

This is equivalent to

$$-av^{(4)} + b\kappa[u_1]v'' = b(\kappa[u_2] - \kappa[u_1])w_2'' + \mathcal{U}(f_1 - f_2).$$

In order to show that $\|v\|_{H^2(x_0,x_1)} \leq q\|\tilde{w}_1 - \tilde{w}_2\|_{H^2(x_0,x_1)}$ for some $q \in (0,1)$, we again want use the Lax-Milgram theorem which gives us that $\|v\|_{H^2(x_0,x_1)}$ is less or equal the the $H_\partial^{2'}$-norm of the right-hand-side, which we therefore have to estimate:

$$\begin{aligned}
&\sup_{\varphi \in H_\partial^2,\, \|\varphi\|_{H^2}=1} \left| \int_{x_0}^{x_1} [b(\kappa[u_2] - \kappa[u_1])w_2''\varphi + \mathcal{U}(f_1 - f_2)]\varphi \, dx \right| \\
&\leq \sup_{\varphi \in H_\partial^2,\, \|\varphi\|_{H^2}=1} \Big\{ b|\kappa[u_2] - \kappa[u_1]| \|w_2''\|_{L^2(x_0,x_1)} \|\varphi\|_{L^2(x_0,x_1)} \\
&\quad + |\mathcal{U}| \|f_1 - f_2\|_{L^2(x_0,x_1)} \|\varphi\|_{L^2(x_0,x_1)} \Big\} \\
&\leq b \underbrace{|\kappa[u_2] - \kappa[u_1]|}_{(*)} \underbrace{\|w_2''\|_{L^2(x_0,x_1)}}_{(**)} + |\mathcal{U}| \underbrace{\|f_1 - f_2\|_{L^2(x_0,x_1)}}_{(***)}
\end{aligned}$$

From the first to the second line we used the Cauchy-Schwarz inequality. Now we will estimate the terms $(*)$, $(**)$ and $(***)$ separately.

We will start with $(*)$ as follows:

$$\begin{aligned}
(*) &= |\kappa[u_2] - \kappa[u_1]| \\
&= \frac{1}{2} \left| \int_{x_0}^{x_1} (u_2'^2 - u_1'^2) \, dx \right| \\
&\leq \frac{1}{2} \int_{x_0}^{x_1} |\tilde{w}_2' - \tilde{w}_1'| \, |2\bar{u}' + \tilde{w}_2' + \tilde{w}_1'| \, dx \\
&\leq \frac{c_1}{2} \|\tilde{w}_2' - \tilde{w}_1'\|_{L^1(x_0,x_1)} \\
&\leq \frac{c_1}{2} \sqrt{x_1 - x_0} \|\tilde{w}_2' - \tilde{w}_1'\|_{L^2(x_0,x_1)} \\
&\leq \frac{c_1}{2} \sqrt{x_1 - x_0} \|\tilde{w}_2 - \tilde{w}_1\|_{H^2(x_0,x_1)}.
\end{aligned}$$

From the third to the fourth line we used that $\bar{u}'$ is constant and $\tilde{w}_1'$ and $\tilde{w}_2'$ are bounded and therefore $|2\bar{u}' + \tilde{w}_2' + \tilde{w}_1'| \leq c_1$, for some constant $c_1 > 0$, while from the fourth to the fifth line we used the Cauchy-Schwarz inequality.

For $(**)$ we use again the estimate (15) we get from the Lax-Milgram theorem.

$$(**) = \|w_2''\|_{L^2(x_0,x_1)} \leq \|w_2\|_{H^2(x_0,x_1)} \leq c|\mathcal{U}|\|f_2\|_{L^2(x_0,x_1)}$$

To estimate $\|f_2\|_{L^2(x_0,x_1)}$ further, we proceed as in (19)-(20) and since we assumed $\tilde{w}_2 \in \mathcal{S}$ we get

$$(**) = \|w_2''\|_{L^2(x_0,x_1)} \leq |\mathcal{U}|c_2 M,$$

for some constant $c_2 > 0$.

In the last step we have to estimate $(***)$. As in (19), we use the definition of f_j and the fact that denominator is greater than one. This yields

$$\begin{aligned}
(***) &= \|f_1 - f_2\|_{L^2(x_0,x_1)} \\
&= \left(\int_{x_0}^{x_1} |f_1(x,\tilde{w}_1,\tilde{w}_1') - f_2(x,\tilde{w}_2,\tilde{w}_2')|^2 \, dx\right)^{\frac{1}{2}} \\
&\leq \left(\int_{x_0}^{x_1} \left|p(x,\tilde{w}_1,\tilde{w}_1')(1+(\bar{u}'+\tilde{w}_2')^2) - p(x,\tilde{w}_2,\tilde{w}_2')(1+(\bar{u}'+\tilde{w}_2')^2)\right|^2 \, dx\right)^{\frac{1}{2}}.
\end{aligned}$$

Next we again use the boundedness of $\tilde{w}_j'$, $j \in \{1,2\}$ and the local Lipschitz continuity of the polynomial. Let therefore L_p be the Lipschitz constant of p in $[x_0,x_1]$ with respect to the second argument, then we get for a suitable constant $c_3 > 0$,

$$\begin{aligned}
(***) &\leq K\left(\int_{x_0}^{x_1} |p(x,\tilde{w}_1,\tilde{w}_1') - p(x,\tilde{w}_2,\tilde{w}_2')|^2 \, dx\right)^{\frac{1}{2}} \\
&\leq c_3 L_p \left(\int_{x_0}^{x_1} |\tilde{w}_1 - \tilde{w}_2|^2 \, dx\right)^{\frac{1}{2}} \\
&= c_3 L_p \|\tilde{w}_1 - \tilde{w}_2\|_{L^2(x_0,x_1)}.
\end{aligned}$$

Finally, putting all this together gives us the desired estimate for the right-hand-side of the equation by

$$\begin{aligned}
&\|w_1 - w_2\|_{H^2(x_0,x_1)} = \|v\|_{H^2(x_0,x_1)} \\
&\leq c_4 \sup_{\varphi \in H^2_\partial,\, \|\varphi\|_{H^2}=1} \left|\int_{x_0}^{x_1} [b(\kappa[u_2]-\kappa[u_1])w_2'' + \mathcal{U}(f_1-f_2)]\varphi \, dx\right| \\
&\leq c_4 \left(|\mathcal{U}|\frac{bc_1c_2M}{2}\sqrt{x_1-x_0}\|\tilde{w}_2-\tilde{w}_1\|_{H^2(x_0,x_1)} + |\mathcal{U}|c_3L_p\|\tilde{w}_1-\tilde{w}_2\|_{L^2(x_0,x_1)}\right) \\
&\leq c_4 \left(|\mathcal{U}|\frac{bc_1c_2M}{2}\sqrt{x_1-x_0}\|\tilde{w}_2-\tilde{w}_1\|_{H^2(x_0,x_1)} + |\mathcal{U}|c_3L_p\|\tilde{w}_1-\tilde{w}_2\|_{H^2(x_0,x_1)}\right) \\
&= \underbrace{|\mathcal{U}|c_4\left(\frac{bc_1c_2M}{2}\sqrt{x_1-x_0} + c_3L_p\right)}_{=:q} \|\tilde{w}_2-\tilde{w}_1\|_{H^2(x_0,x_1)}.
\end{aligned}$$

With $|\mathcal{U}|$ sufficiently small we achieve

$$q := |\mathcal{U}| c_4 \left(\frac{b c_1 c_2 M}{2} \sqrt{x_1 - x_0} + c_3 L_p \right) < 1, \tag{21}$$

which assures that the mapping G is a contraction and therefore, we get the convergence of our fixed-point iteration given by $w_{n+1} := G(w_n)$. We generated a function $w \in \mathcal{S}$, $w = \lim_{n\to\infty} w_n$, which solves the problem (11). Therefore, $\bar{u} + w$ is the unique solution to our original problem (7).
Proceeding with the bootstrapping arguments in section 1.2, we end up with a solution $w \in C^\infty[x_0, x_1]$.

Theorem 3 (Existence and uniqueness of a solution)**.** *Let q be defined as in (21) and $\mathcal{U} < 0$ chosen such that $q < 1$.*
Then there exists a unique classical solution $w \in C^\infty[x_0, x_1]$ to the problem (11).

Part 4. Numerical Simulations

In this last chapter, we present some numerical simulations of our simplified quasi-stationary model (7). Therefore, we use the methods and results form the previous chapter. This means that we produce a fixed-point sequence by solving the linear problem (13) with constant curvature and independent right-hand-side in each iteration step. From the solution we calculate the curvature and the nonlinearity which serves as input for the next step.
The implementations are written in MatLab and the code can be found in the appendix.

1. The Algorithm

Following the procedure of the last chapter, the algorithm works as follows:

Algorithm 1 Fixed-point iteration

- **STEP1:** Choose appropriate values for the constants μ, ζ, $\gamma^{\perp}$ and $\mathcal{U}$ of the differential equation in (7), for the endpoints x_0, x_1 of the interval as well as for the boundary value u_0.
- **STEP2:** Choose starting values κ^0 for the curvature and $nonlin^0$ for the nonlinearity on the right-hand-side of the differential equation. Fix $\varepsilon > 0$.
- **STEP3:** Determine w_1 as solution to the linear problem with homogeneous boundary conditions, (13), for the chosen values κ^0 and $f = \frac{nonlin^0}{2\gamma^{\perp}}$.
  Calculate κ^1, using (10) and $nonlin^1$, using (8) resp. (9).
- **STEP4:** Determine w_2 as solution to (13), for the values κ^1 and $f = \frac{nonlin^1}{2\gamma^{\perp}}$.
  Calculate κ^2, using (10) and $nonlin^2$, using (8) resp. (9).
  Set $n = 2$.
- **STEP5:** **If** $\|w_{n-1} - w_n\| \leq \varepsilon$ **then** stop. (*a-posteriori* error estimate)
  Calculate the solution $u(x) = w_n(x) + \frac{u_0}{x_1 - x_0}(x_1 - x)$ for $x \in [x_0, x_1]$.
- **STEP6:** Determine w_{n+1} as solution to (13), for the values κ^n and $f = \frac{nonlin^n}{2\gamma^{\perp}}$.
  Calculate κ^{n+1}, using (10) and $nonlin^{n+1}$, using (8) resp. (9).
  Set $n = n + 1$.
  Got to **STEP5**.

The files `run_fpsqrt.m` and `run_fbftrt.m` contain the implementations of this algorithm, depending on whether one uses v_{sqrt} or v_{ftrt} as velocity field of the blood flow.

2. Methods

In this section we shortly discuss the method used to solve the linear problem (13) in each iteration step. Theoretical background can be found,

for example in [2].

The equation in (13) is a linear fourth order ordinary differential equation. The aim is to replace the ODE by a set of algebraic equations, which can be solved by inverting a sparse matrix. Therefore we will perform *finite difference approximations* of the occurring derivatives. This means that after choosing suitable grid points of the domain, the derivatives are replaced by relationships between the function values at the the nodal points corresponding to the chosen grid.
Since our domain is one-dimensional, the grid simply is given by a subdivision of the interval $[x_0, x_1]$. We will choose an equidistant subdivision $x_0 = x^0 < x^1 < \cdots < x^N = x_1$ for $N \in \mathbb{N}$, with distance $\Delta x := x^i - x^{i-1}$. By $w^i := w(x^i)$, $0 \leq i \leq N$, we denote the nodal points of the solution w. Note that our boundary conditions give us $w^0 = w^N = 0$. Using Taylor expansion, we get

$$w^{i+1} = w^i + \Delta x w'(x^i) + O(\Delta x^2),$$

and after reformulation

$$w'(x^i) = \frac{w^{i+1} - w^i}{\Delta x} + O(\Delta x).$$

This yields the *forward difference approximation* for the first derivative

$$w'(x^i) \sim \frac{w^{i+1} - w^i}{\Delta x}. \tag{22}$$

The remainder term, which is of order Δx, is called the *local truncation error* and will tend to zero as N is chosen bigger.
Using the above approximation (22) consecutively, we get for the derivatives up to order four

$$w''(x^i) \sim \frac{w^{i+1} - 2w^i + w^{i-1}}{\Delta x^2}, \tag{23}$$

$$w'''(x^i) \sim \frac{w^{i+2} - 3w^{i+1} + 3w^i - w^{i-1}}{\Delta x^3}, \tag{24}$$

$$w^{(4)}(x^i) \sim \frac{w^{i+2} - 4w^{i+1} + 6w^i - 4w^{i-1} + w^{i-2}}{\Delta x^4}, \tag{25}$$

for $i \in \{2, \ldots, N-1\}$.
Inserting this in the differential equation in (13) gives us the desired algebraic equations for the nodal points w^i. Since the derivatives occur linear, the left-hand-side can be expressed in terms of matrices. Lets denote the solution vector by $W := (w^0, \ldots, w^N)$ and the solution vector without the first and the last component by $\tilde{W} := (w^1, \ldots, w^{N-1})$. After embedding the information from the values of the second derivative at the boundary points, the left-hand-side reads

$$-\frac{a}{\Delta x^4} A\tilde{W} + \frac{(b\kappa + c)}{\Delta x^2} B\tilde{W},$$

with

$$A = \begin{pmatrix} 5 & -4 & 1 & 0 & & & \dots & 0 \\ -4 & 6 & -4 & 1 & 0 & & \dots & 0 \\ 1 & -4 & 6 & -4 & 1 & 0 & \dots & 0 \\ \vdots & & & \ddots & & & & \vdots \\ 0 & \dots & 0 & 1 & -4 & 6 & -4 & 1 \\ 0 & \dots & & 0 & 1 & -4 & 6 & -4 \\ 0 & \dots & & & 0 & 1 & -4 & 5 \end{pmatrix} \in \mathbb{R}^{N-1 \times N-1},$$

and

$$B = \begin{pmatrix} -2 & 1 & 0 & & \dots & 0 \\ 1 & -2 & 1 & 0 & \dots & 0 \\ \vdots & & \ddots & & & \vdots \\ 0 & \dots & 0 & 1 & -2 & 1 \\ 0 & \dots & & 0 & 1 & -2 \end{pmatrix} \in \mathbb{R}^{N-1 \times N-1}.$$

Keeping in mind that we have homogeneous boundary conditions, the linear system approximating the differential equation is given by

$$-\frac{a}{\Delta x^4} A\tilde{W} + \frac{(b\kappa + c)}{\Delta x^2} B\tilde{W} = \mathcal{U}F, \tag{26}$$

where we denote by

$$F := \begin{pmatrix} f(x^1) \\ \vdots \\ f(x^{N-1}) \end{pmatrix} \in \mathbb{R}^{N-1}$$

the vector of the given right-hand-side at the nodal points.
$\tilde{W}$ and hence the solution W can be determined explicitly by inverting the nonsingular matrix

$$-\frac{a}{\Delta x^4} A + \frac{(b\kappa + c)}{\Delta x^2} B.$$

The file `solvelin.m` in the appendix contains the implementation of the above described finite difference method to solve (13) numerically.

3. Simulation Results

In this last section results and outcomes of simulations under some scenarios are shown. The aim was to investigate how the choice of the different parameters, especially the speed of the blood flow $\mathcal{U}$, influence the convergence behavior of the fixed-point iteration and the deflection of the solution u from the interpolation $\bar{u}$. Here we have to mention that the values chosen for the constants should only be seen relatively to each other and do not originate from experiments. Furthermore, the difference between the two velocity fields of the blood flow, v_{sqrt} and v_{ftrt} was examined.

Four graphics are produced by the simulations. The most important picture shows the tether, the interpolation and the velocity field of the blood flow combined in one plot. Moreover, also a plot of the H^2-norm of the elements of the fixed-point sequence with respect to the steps is generated and the arc-length respectively L^2-norm of the nonlinearity are plotted against the steps.

For the presented results, we chose the following values for the parameters:

constant	value
μ	0.1
ζ	1
$\gamma^{\perp}$	7
N	1000
ε	10^{-4}

As starting value for the curvature the length of the interpolation, $\kappa^0 = \sqrt{5}$, and for the nonlinearity the vector $nonlin^0 = (1, \ldots, 1) \in \mathbb{R}^N$ was chosen.

Simulations using the velocity field v_{sqrt}: We set $x_0 = 0$, $x_1 = 1$ and $u_0 = 2$ and compare the cases $\mathcal{U} = -0.9$ and $\mathcal{U} = -2.5$. The corresponding plots can be found in 9-12.
The first thing to say is that in case of a higher speed $\mathcal{U}$ more iteration steps are needed. It takes 8 iterations to fulfill the stopping criterion in the case $\mathcal{U} = -0.9$ and 21 for $\mathcal{U} = -2.5$. This of course coincides with our analytical results, since a higher speed causes a bigger contraction constant and therefore slower convergence. At some critical value of $\mathcal{U}$, which we did not compute explicitly, the convergence of the fixed-point iteration can no longer be provided. In this scenario, it can be assumed that the critical value is about $\mathcal{U} = -5.66$. For $\mathcal{U} = -5.6$ it takes 49 and for $\mathcal{U} = -5.65$ 235 steps until the stopping criterion is achieved. For values beyond -5.65 we stopped the algorithm after 6000 iterations.
As expected, we can also observe that the higher $\mathcal{U}$ gets the more the tether bends under the force of the blood flow. In 9 one can see that in the first case 9(a) the tether does not move far away from the interpolation line, while in the second case 9(b) displacement can be noticed clearly.

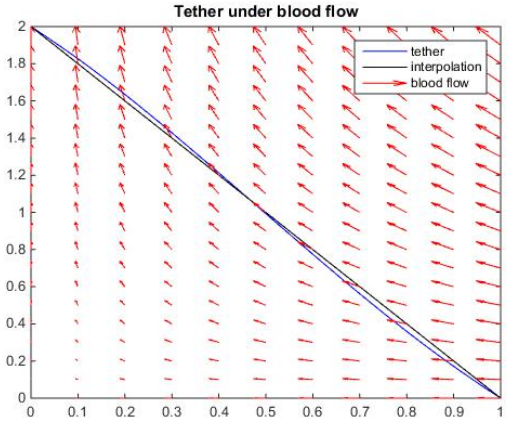

(a) Speed of the blood flow $\mathcal{U} = -0.9$

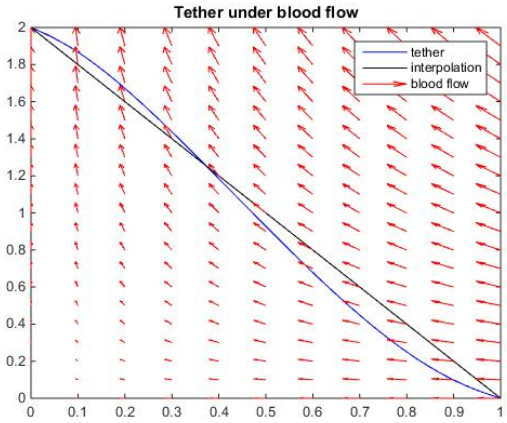

(b) Speed of the blood flow $\mathcal{U} = -2.5$

FIGURE 9. Tether under blood flow for $v = v_{sqrt}$

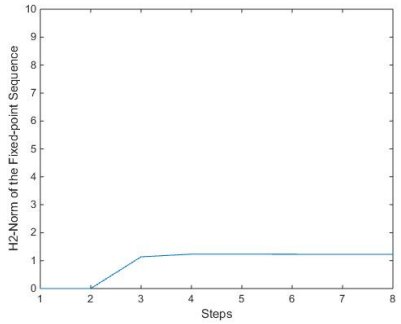

(a) Speed of the blood flow $\mathcal{U} = -0.9$

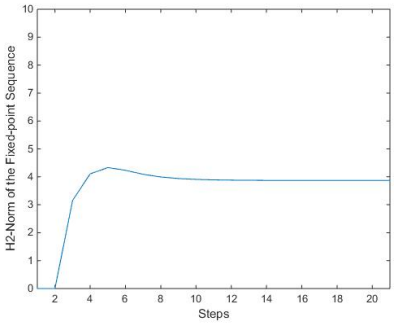

(b) Speed of the blood flow $\mathcal{U} = -2.5$

FIGURE 10. H^2-norm of the fixed-point sequence

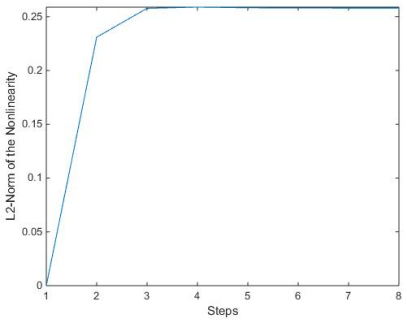

(a) Speed of the blood flow $\mathcal{U} = -0.9$

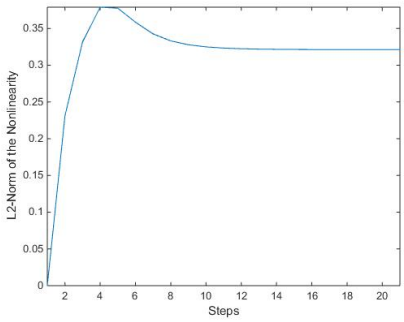

(b) Speed of the blood flow $\mathcal{U} = -2.5$

FIGURE 11. L^2-norm of the nonlinearity

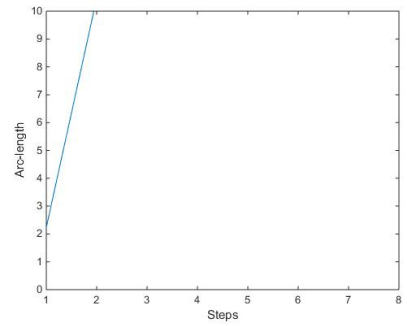

(a) Speed of the blood flow $\mathcal{U} = -0.9$

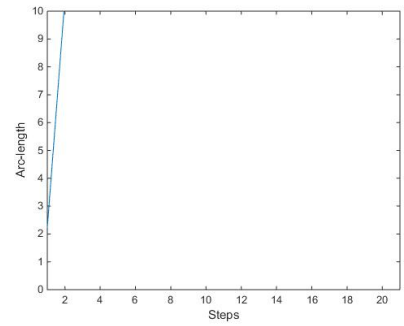

(b) Speed of the blood flow $\mathcal{U} = -2.5$

FIGURE 12. Arc-length

Simulations using the velocity field v_{ftrt}: We set $x_0 = 0.3$, $x_1 = 1$ and $u_0 = x_0\sqrt{5-\sqrt{20}}$ and compare the cases $\mathcal{U} = -0.3$ and $\mathcal{U} = -0.9$. The corresponding plots can be found in 13-16.
Again, we can observe a little increase of the iterations as the speed $\mathcal{U}$ is chosen higher. For $\mathcal{U} = -0.3$ 10 steps are needed while for $\mathcal{U} = -0.9$ the stopping criterion is fulfilled after 14 steps. After some numerical tests, it may be assumed that the critical value for convergence lies about $\mathcal{U} = -1.6$, which is a lot lower than in the case where we used v_{sqrt}. But for biologically meaningful simulations, only $\mathcal{U} > -1$ should be considered, since otherwise there occur function values of the solution which lie above the line $\left\{(x,y) \in [0,\infty) \times [0,\infty) \ : \ y = x\sqrt{5-\sqrt{20}}\right\}$ and therefore, the tether leaves the relevant area. Biologically, this means that the displacement of the tether from the interpolation line is that strong that it would be pressed against the neutrophil. An example of such a case can be seen in 17 where we chose $\mathcal{U} = -1.3$ and the stopping criterion was achieved after 21 steps.

If we compare the results where we used v_{sqrt} to the ones with v_{ftrt}, we see that the generated sequence converges faster in the first case, where the

polynomial contained in the nonlinearity is of less degree. For $\mathcal{U} = -0.9$ 14 steps are needed to fulfill the stopping criterion with the right-hand-side containing v_{ftrt}, while in the case with v_{sqrt} only 8 steps were sufficient. The difference of the needed iterations increases as the speed of the blood flow does.

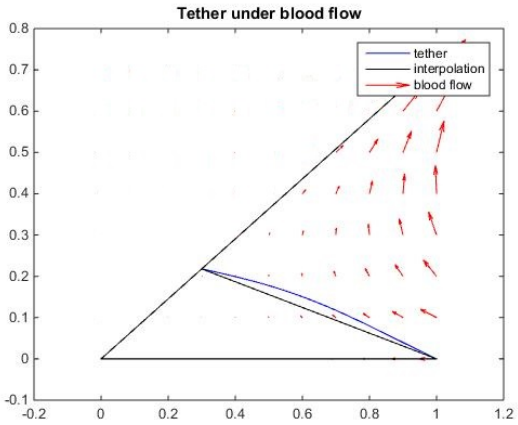

(a) Speed of the blood flow $\mathcal{U} = -0.3$

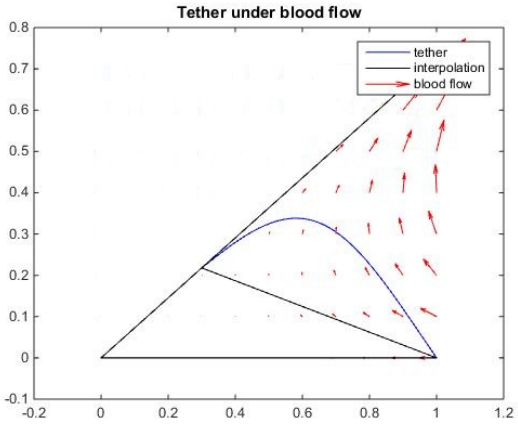

(b) Speed of the blood flow $\mathcal{U} = -0.9$

FIGURE 13. Tether under blood flow for $v = v_{ftrt}$

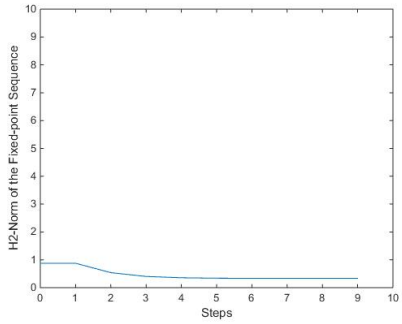

(a) Speed of the blood flow $\mathcal{U} = -0.3$

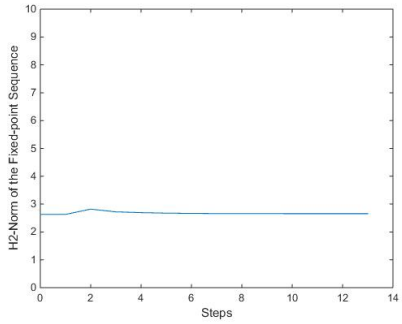

(b) Speed of the blood flow $\mathcal{U} = -0.9$

FIGURE 14. H^2-norm of the fixed-point sequence

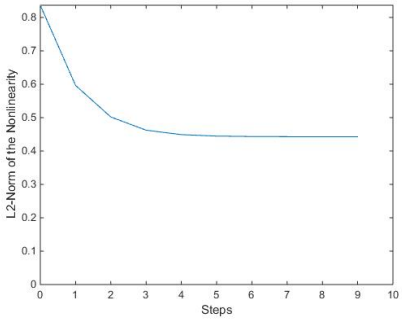

(a) Speed of the blood flow $\mathcal{U} = -0.3$

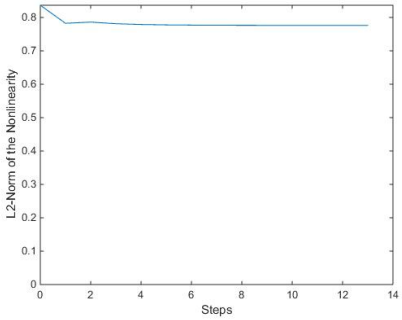

(b) Speed of the blood flow $\mathcal{U} = -0.9$

FIGURE 15. L^2-norm of the nonlinearity

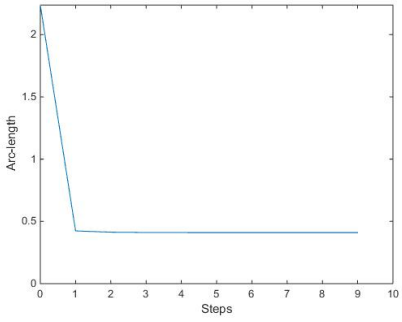

(a) Speed of the blood flow $\mathcal{U} = -0.3$

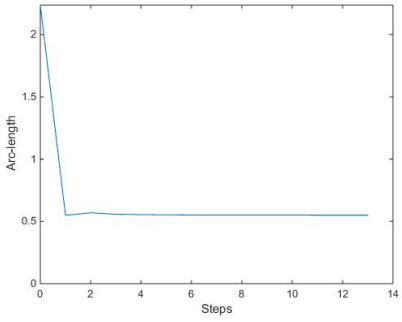

(b) Speed of the blood flow $\mathcal{U} = -0.9$

FIGURE 16. Arc-length

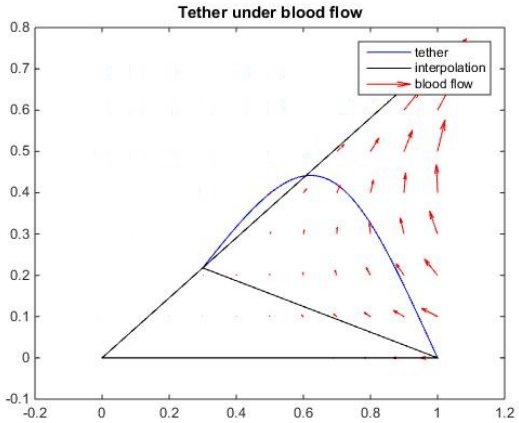

FIGURE 17. Tether exceeds relevant area for $\mathcal{U} = -1.3$

Part 5. Outlook

The results in this work can be seen as first attempt to model a tether under the forces it has to bear from the blood flow and internal tension. Of course this is expandable, the model could be improved and further phenomena could be included.
The first thing to mention is that both the analysis and the numerical simulations of the time dependent problem should also be considered. As a possible next step, one could try to do the computations with a more realistic flow profile of the blood stream near the neutrophil. Since also the streamlines on the left and right of the cell contribute in the behavior of the tether, a corresponding model in 3 dimensions should be developed in order to get more realistic results.
Another interesting phenomenon is the occurrence of tether-breaking. The questions about when this happens, how the tether behaves after getting loose and under which circumstances a tether-to-sling transition is possible could be investigated mathematically by the developing the above model further.

References

[1] H. Brezis *Functional Analysis, Sobolev Spaces and Partial Differential Equations*, Springer, 2011.

[2] G. Evans, J. Blackledge, P. Yardley *Numerical Methods for Partial Differential Equations*, Springer, 2000

[3] E. Kolaczkowska, P. Kubes *Neutrophil recruitment and function in health and inflammation*, Nat. Rev. Immunol., 2013, Vol. **13**(3): p.159

[4] A. Marki, E.Guiterrez, Z. Mikulski, A. Groisman, K.Ley *Microfluidics-based side view flow chamber reveals tether-to-sling transition in rolling neutrophils*, Scientific Reports Vol. 6, published online first 2016

[5] L. Nirenberg *On elliptic partial differential equations*, Annali della Scuola Normale Superiore di Pisa, Classe di Scienze 3e serie, tome 13, n2 (1959), p. 115-162.

[6] C. Schmeiser *Angewandte Mathematik*, Skriptum zur Vorlesung

[7] P. Sundd, M.K. Pospieszalska, L.S. Cheung, K. Konstantopoulos, K. Ley *Biomechanics of leukocyte rolling*, Biorheology. 2011;48(1):1–35

Appendix A. Matlab Code

Solving the Linear Problem

```
function [ w, dw, ddw, VX, delta, kappa0 ] = solvelin( m,g,s,U,x0,x1,u0,N,kappa,nonlin )

%%%%%%%%%%%%%%%%%%%%%%%%%%%%%%%%%%%%%%%%%%%%%%%%%%%%%%%%%%%%%%%%%%%%%%%%%%%%
% Solves the linear boundary value problem:                               %
%                                                                          %
% -a*w^(4)+(b*kappa+c)*w^(2)=U*2*g*nonlin,                                 %
% w(x0)=w(x1)=0,                                                           %
% w^(2)(x0)=w^(2)(x1)=0,                                                   %
%                                                                          %
% with finite difference method.                                           %
%%%%%%%%%%%%%%%%%%%%%%%%%%%%%%%%%%%%%%%%%%%%%%%%%%%%%%%%%%%%%%%%%%%%%%%%%%%%

VX=linspace(x0,x1,N+1); %subdivision of the interval
delta=VX(2)-VX(1); %length of subdivision-intervals
kappa0=sqrt((x1-x0)^2+u0^2); %interpolation arclength
w=zeros(N+1,1); %initialization of solution vector
A=sparse(N-1,N-1); %initialization of matrix
B=sparse(N-1,N-1); %initialization of matrix
dw=zeros(N,1); %initialization of the derivative of the solution
ddw=zeros(N,1); %initialization of the second derivative of the solution

%definition of the constants
a=m*((x1-x0)/kappa0)^4;
b=s*((x1-x0)/kappa0)^2;

%definition of the left-hand-side
for i=1:N-1
    B(i,i)=-2;
end

A(1,1)=5;
A(N-1,N-1)=5;

for i=2:N-2
    A(i,i)=6;
end

for i=1:N-2
    B(i,i+1)=1;
    B(i+1,i)=1;
    A(i,i+1)=-4;
    A(i+1,i)=-4;
end

for i=1:N-3
    A(i,i+2)=1;
    A(i+2,i)=1;
end

M=-a*(1/delta^4)*A+b*kappa*(1/delta^2)*B;

%definition of the right-hand-side (keeping in mind that we have
%homogeneous boundary conditions)
rhs=2*g*U*nonlin(1:N-1);

%solving the system M*w(2:N)=rhs
w(2:N)=M\rhs;

%computing the derivative, dw
for i=1:N
    dw(i)=(w(i+1)-w(i))/delta;
end

%computing the second derivative, ddw
ddw(1)=0;
```

```
66 for  i=2:N
67      ddw(i)=(w(i+1)-2*w(i)+w(i-1))/delta^2;
68 end
69
70 end
```

Fixed-Point Iteration for $nonlin_{sqrt}$

```
%%%%%%%%%%%%%%%%%%%%%%%%%%%%%%%%%%%%%%%%%%%%%%%%%%%%%%%%%%%%%%%%%%%%%%%%%%%%%%%%
% Executes a fixed-point iteration by solving the linear boundary value    %
% problem:                                                                   %
%                                                                            %
% -a*w^(4)+(b*kappa+c)*w^(2)=U*2*g*nonlin_sqrt,                              %
% w(x0)=w(x1)=0,                                                             %
% w^(2)(x0)=w^(2)(x1)=0,                                                     %
%                                                                            %
% with solvelin.m in each step for given and fixed a, b, c, g (calculated %
% from the constants) and input kappa and nonlin_sqrt.                       %
%                                                                            %
% Plots the 2-norm of the solutions of solvelin.m, kappa and the 2-norm   %
% of nonlin_sqrt with respect to the steps.                                  %
% Plots the interpolation bu and the solution u=bu+w together with the    %
% velocity field of the bloodflow, given by v=2*U*(a,-b).                   %
%%%%%%%%%%%%%%%%%%%%%%%%%%%%%%%%%%%%%%%%%%%%%%%%%%%%%%%%%%%%%%%%%%%%%%%%%%%%%%%%

%% Constants

m=0.1; %elasticity coefficient in transverse direction
s=1; %proportionality constant of elongation
g=7; %friction coefficient
U=-2.5; %velocitiy of the bloodflow
x0=0; %left boundary
x1=1; %right boundary
u0=2; %endpoint on granulocyte
N=1000; %number of subdivision points of the interval


%% First two iteration steps

kappa=sqrt(5); %startingvalue of the curvature
nonlin=zeros(N,1); %startingvector of the nonliniarity

%%Step 1
%solve
[w,dw,ddw,x,delta,kappa0]=solvelin( m,g,s,U,x0,x1,u0,N,kappa,nonlin);

%define bu (interpolation)
bu=zeros(N+1,1);
for i=1:N+1
    bu(i)=(u0*(x1-x(i)))/(x1-x0);
end
dbu=-u0/(x1-x0); %derivative of bu, constant

solutionnorm=sqrt(delta)*sqrt(norm(w)^2+norm(dw)^2+norm(ddw)^2); %vector
    storing the approximation of the H2-norm of the solution in each
    iteration step
arclength=kappa; %vector storing the arclength of the solution in each
    iteration step
rhs=sqrt(delta)*norm(nonlin); %vector storing the approximation of the L2-
    norm of the nonlinearity in each iteration step

%calculating (approximating) the curvature-integral for the next step
sum=0;
for i=1:N
    sum=sum+(dbu+dw(i))^2;
end
kappa=((u0^4+(x1-x0)^4+(3/2)*u0^2*(x1-x0)^2)/kappa0)+((x1-x0)^3/(2*kappa0
    ^3))*delta*sum;

%calculating the nonlinearity for the next step
for i=1:N
    nonlin(i)=(bu(i)+w(i)+x(i)*dbu+x(i)*dw(i))/(1+(dbu+dw(i))^2);
end

%%Step 2
```

```
63 solutionnorm=[solutionnorm,sqrt(delta)*sqrt(norm(w)^2+norm(dw)^2+norm(ddw)
       ^2)];
64 arclength=[arclength,kappa];
65 rhs=[rhs,sqrt(delta)*norm(nonlin)];
66 wold=w;
67 dwold=dw;
68 ddwold=ddw;
69 %solve
70 [w,dw,ddw,x,delta,kappa0]=solvelin( m,g,s,U,x0,x1,u0,N,kappa,nonlin);
71
72 %calculating (approximating) the curvature-integral for the next step
73 sum=0;
74 for i=1:N
75     sum=sum+(dbu+dw(i))^2;
76 end
77 kappa=((u0^4+(x1-x0)^4+(3/2)*u0^2*(x1-x0)^2)/kappa0)+((x1-x0)^3/(2*kappa0
       ^3))*delta*sum;
78
79 %calculating the nonlinearity for the next step
80 for i=1:N
81     nonlin(i)=(bu(i)+w(i)+x(i)*dbu+x(i)*dw(i))/(1+(dbu+dw(i))^2);
82 end
83
84 %% Loop over kappa and nonlin (fixedpoint iteration)
85 steps=2;
86 while(sqrt(delta)*sqrt(norm(w(1:N)-wold(1:N))^2+norm(dw-dwold)^2+norm(ddw-
       ddwold)^2)>0.0001 && steps<6000)
87
88     steps=steps+1;
89     solutionnorm=[solutionnorm,sqrt(delta)*sqrt(norm(w)^2+norm(dw)^2+norm(
       ddw)^2)];
90     arclength=[arclength,kappa];
91     rhs=[rhs,sqrt(delta)*norm(nonlin)];
92     wold=w;
93     dwold=dw;
94     ddwold=ddw;
95
96     %solve
97     [w,dw,ddw,x,delta,kappa0]=solvelin(m,g,s,U,x0,x1,u0,N,kappa,nonlin);
98
99     %calculating the curvature for the next step
100    sum=0;
101    for i=1:N
102    sum=sum+(dbu+dw(i))^2;
103    end
104
105    kappa=((u0^4+(x1-x0)^4+(3/2)*u0^2*(x1-x0)^2)/kappa0)+((x1-x0)^3/(2*
       kappa0^3))*delta*sum;
106
107    %calculating the nonlinearity for the next step
108    for i=1:N
109    nonlin(i)=(bu(i)+w(i)+x(i)*dbu+x(i)*dw(i))/(1+(dbu+dw(i))^2);
110    end
111
112 end
113
114 u=bu+w; %original solution u is the interpolation bu + the perturbation w
115
116 st=['Steps:',num2str(steps)];
117 disp(st);
118
119 %%% Plots
120
121 %plots the 2-norm of the solution in each step
122 figure
123 plot(1:1:steps,solutionnorm);
124 axis([1 steps 0 10]);
125 xlabel('Steps');
126 ylabel('H2-Norm of the Fixed-point Sequence');
127
```

```
128 %plots the arclength in each step
129 figure
130 plot(1:1:steps,arclength);
131 axis([1 steps 0 10]);
132 xlabel('Steps');
133 ylabel('Arc-length');
134
135 %plots the 2-norm of the nonlinearity in each step
136 figure
137 plot(1:1:length(rhs),rhs);
138 axis([1 steps 0 max(rhs)]);
139 xlabel('Steps');
140 ylabel('L2-Norm of the Nonlinearity');
141
142 %plots the tether(u), the interpolation (bu) and the velocity field of the
143 %bloodflow
144 figure
145 plot(x,u,'b');
146 [a,b]=meshgrid(0:0.1:x1,min(u):0.1:max(u));
147
148 hold on;
149 plot(x,bu,'k');
150 quiver(a,b,2*U*a,-2*U*b,'r');
151 axis([0 x1 min(u) max(u)]);
152 hold off;
153 legend('tether','interpolation','blood flow');
154 title('Tether under blood flow');
```

Fixed-Point Iteration for $nonlin_{ftrt}$

```
%%%%%%%%%%%%%%%%%%%%%%%%%%%%%%%%%%%%%%%%%%%%%%%%%%%%%%%%%%%%%%%%%%%%%%%%%%%
% Executes a fixed-point iteration by solving the linear boundary value   %
% problem:                                                                %
%                                                                         %
% -a*w^(4)+(b*kappa+c)*w^(2)=U*2*g*nonlin_ftrt,                           %
% w(x0)=w(x1)=0,                                                          %
% w^(2)(x0)=w^(2)(x1)=0,                                                  %
%                                                                         %
% with solvelin.m in each step for given and fixed a, b, c, g (calculated %
% from the constants) and input kappa and nonlin_ftrt.                    %
%                                                                         %
% Plots the 2-norm of the solutions of solvelin.m, kappa and the 2-norm   %
% of nonlin_ftrt with respect to the steps.                               %
% Plots the interpolation bu and the solution u=bu+w together with the    %
% velocity field of the bloodflow, given by                               %
% v=2*U*(5*a^4-30*a^2*b^2+5*b^4,-20*a^3*b+20*a*b^3).                      %
%%%%%%%%%%%%%%%%%%%%%%%%%%%%%%%%%%%%%%%%%%%%%%%%%%%%%%%%%%%%%%%%%%%%%%%%%%%

%% Constants

m=0.1; %elasticity coefficient in transverse direction
s=1; %proportionality constant of elongation
g=7; %friction coefficient
U=-0.9; %velocitiy of the bloodflow
x0=0.3; %left boundary
x1=1; %right boundary
u0=x0*sqrt(5-sqrt(20)); %endpoint on granulocyte
N=1000; %number of subdivision points of the interval

%% First two iteration steps

kappa=sqrt(5); %startingvalue of the curvature
nonlin=ones(N,1); %startingvector of the nonliniarity


%step1
%solve
[w,dw,ddw,x,delta,kappa0]=solvelin( m,g,s,U,x0,x1,u0,N,kappa,nonlin );

%define bu (interpolation)
bu=zeros(N+1,1);
for i=1:N+1
    bu(i)=(u0*(x1-x(i)))/(x1-x0);
end
dbu=-u0/(x1-x0); %derivative of bu, constant

solutionnorm=sqrt(delta)*sqrt(norm(w)^2+norm(dw)^2+norm(ddw)^2); %vector storing the approximation of the H2-norm of the solution in each iteration step
arclength=kappa; %vector storing the arclength of the solution in each iteration step
rhs=sqrt(delta)*norm(nonlin); %vector storing the approximation of the L2-norm of the nonlinearity in each iteration step

%calculating (approximating) the curvature-integral for the next step
sum=0;
for i=1:N
    sum=sum+(dbu+dw(i))^2;
end
kappa=((u0^4+(x1-x0)^4+(3/2)*u0^2*(x1-x0)^2)/kappa0)+((x1-x0)^3/(2*kappa0^3))*delta*sum;


%calculating the nonlinearity for the next step
nonlin=zeros(N-1,1);
for i=1:N
```

```
62      nonlin(i)=(5*x(i)^4*(dbu+dw(i))+5*(bu(i)+w(i))^4*(dbu+dw(i))-30*x(i)
        ^2*(bu(i)+w(i))^2*(dbu+dw(i))+20*x(i)^3*(bu(i)+w(i))-20*x(i)*(bu(i)+w(i
        ))^3)/(1+(dbu+dw(i))^2);
63  end
64
65  %Step 2
66  solutionnorm=[solutionnorm,sqrt(delta)*sqrt(norm(w)^2+norm(dw)^2+norm(ddw)
        ^2)];
67  arclength=[arclength,kappa];
68  rhs=[rhs,sqrt(delta)*norm(nonlin)];
69  wold=w;
70  dwold=dw;
71  ddwold=ddw;
72
73  %solve
74  [w,dw,ddw,x,delta,kappa0]=solvelin( m,g,s,U,x0,x1,u0,N,kappa,nonlin );
75
76  %calculating (approximating) the curvature-integral for the next step
77  sum=0;
78  for i=1:N
79      sum=sum+(dbu+dw(i))^2;
80  end
81  kappa=((u0^4+(x1-x0)^4+(3/2)*u0^2*(x1-x0)^2)/kappa0)+((x1-x0)^3/(2*kappa0
        ^3))*delta*sum;
82
83
84  %calculating the nonlinearity for the next step
85  nonlin=zeros(N-1,1);
86  for i=1:N
87      nonlin(i)=(5*x(i)^4*(dbu+dw(i))+5*(bu(i)+w(i))^4*(dbu+dw(i))-30*x(i)
        ^2*(bu(i)+w(i))^2*(dbu+dw(i))+20*x(i)^3*(bu(i)+w(i))-20*x(i)*(bu(i)+w(i
        ))^3)/(1+(dbu+dw(i))^2);
88  end
89
90  %% Loop over kappa and nonlin (fixed-point iteration)
91  steps=2;
92  while(sqrt(delta)*sqrt(norm(w(1:N)-wold(1:N))^2+norm(dw-dwold)^2+norm(ddw-
        ddwold)^2)>0.0001 && steps<6000)
93
94      steps=steps+1;
95      solutionnorm=[solutionnorm,sqrt(delta)*sqrt(norm(w)^2+norm(dw)^2+norm(
        ddw)^2)];
96      arclength=[arclength,kappa];
97      rhs=[rhs,sqrt(delta)*norm(nonlin)];
98      wold=w;
99      dwold=dw;
100     ddwold=ddw;
101
102     %solve
103     [w,dw,ddw,x,delta,kappa0]=solvelin( m,g,s,U,x0,x1,u0,N,kappa,nonlin );
104
105     %calculating (approximating) the curvature-integral for the next step
106     sum=0;
107     for i=1:N
108      sum=sum+(dbu+dw(i))^2;
109     end
110     kappa=((u0^4+(x1-x0)^4+(3/2)*u0^2*(x1-x0)^2)/kappa0)+((x1-x0)^3/(2*
        kappa0^3))*delta*sum;
111
112
113 %calculating the nonlinearity for the next step
114     nonlin=zeros(N-1,1);
115     for i=1:N
116      nonlin(i)=(5*x(i)^4*(dbu+dw(i))+5*(bu(i)+w(i))^4*(dbu+dw(i))-30*x(i)
        ^2*(bu(i)+w(i))^2*(dbu+dw(i))+20*x(i)^3*(bu(i)+w(i))-20*x(i)*(bu(i)+w(i
        ))^3)/(1+(dbu+dw(i))^2);
117     end
118
119 end
120
```

```
121 u=bu+w; %original solution u is the interpolation bu + the perturbation w
122
123 st=['Steps:',num2str(steps)];
124 disp(st);
125
126 %% Plots
127
128 %plots the H2-norm of the solution in each step
129 plot(0:1:steps-1,solutionnorm);
130 axis([0 steps 0 10]);
131 xlabel('Steps');
132 ylabel('H2-Norm of the Fixed-point Sequence');
133 figure
134
135 %plots the arclength in each step
136 plot(0:1:steps-1,arclength);
137 axis([0 steps 0 max(arclength)]);
138 xlabel('Steps');
139 ylabel('Arc-length');
140 figure
141
142 %plots the L2-norm of the nonlinearity in each step
143 plot(0:1:length(rhs)-1,rhs);
144 axis([0 steps 0 max(rhs)]);
145 xlabel('Steps');
146 ylabel('L2-Norm of the Nonlinearity');
147 figure
148
149 %plots the tether (u), the interpolation (bu) and the velocity field of the
150 %bloodflow
151 plot(x, u,'b');
152
153 [a,b]=meshgrid(0:0.1:x1,min(u):0.1:(x1*sqrt(5-sqrt(20))));
154
155 hold on
156 plot(x,bu,'k');
157 quiver(a,b,U*(5*a.^4-30*a.^2.*b.^2+5*b.^4),U*(-20*a.^3.*b+20*a.*b.^3),'r');
158 plot(a(1,:),zeros(length(a(1,:)))','k');
159 plot(a(1,:),a(1,:)*sqrt(5-sqrt(20)),'k');
160 hold off
161 legend('tether','interpolation','blood flow');
162 title('Tether under blood flow');
```